crystals

MDPI

Review

Recent Progress of Film Fabrication Process for Carbon-Based All-Inorganic Perovskite Solar Cells

Haifeng Yang [1], Hui Wang [2,*], Ke Wang [3], Dongqi Liu [1], Lifang Zhao [2], Dazheng Chen [4], Weidong Zhu [4], Jincheng Zhang [4] and Chunfu Zhang [4,*]

1 College of Physics and Optoelectronics Technology, Baoji University of Arts and Sciences, Baoji 721016, China; yanghaifeng@bjwlxy.edu.cn (H.Y.); ldq15286691436@163.com (D.L.)
2 Shaanxi Key Laboratory of Phytochemistry, College of Chemistry and Chemical Engineering, Baoji University of Arts and Science, Baoji 721013, China; zlfzhao@163.com
3 North Automatic Control Technology Institute, Taiyuan 030006, China; 13623465815@163.com
4 Wide Bandgap Semiconductor Technology Disciplines State Key Laboratory, School of Microelectronics, Xidian University, Xi'an 710071, China; dzchen@xidian.edu.cn (D.C.); wdzhu@xidian.edu.cn (W.Z.); jchzhang@xidian.edu.cn (J.Z.)
* Correspondence: wangkejian@163.com (H.W.); cfzhang@xidian.edu.cn (C.Z.)

Abstract: Although the certified power conversion efficiency of organic-inorganic perovskite solar cells (PSCs) has reached 25.7%, their thermal and long-term stability is a major challenge due to volatile organic components. This problem has been a major obstacle to their large-scale commercialization. In the last few years, carbon-based all-inorganic perovskite solar cells (C−IPSCs) have exhibited high stability and low-cost advantages by adopting the all-inorganic component with cesium lead halide ($CsPbI_{3-x}Br_x$, x = 0 ~ 3) and eliminating the hole-transporting layer by using cheap carbon paste as the back electrode. So far, many astonishing developments have been achieved in the field of C−IPSCs. In particular, the unencapsulated $CsPbBr_3$ C-IPSCs exhibit excellent stability over thousands of hours in an ambient environment. In addition, the power conversion efficiencies of $CsPbI_3$ and $CsPbI_2Br$ C-IPSCs have exceeded 15%, which is close to that of commercial multicrystalline solar cells. Obtaining high-quality cesium lead halide-based perovskite films is the most important aspect in the preparation of high-performance C-IPSCs. In this review, the main challenges in the high-quality film fabrication process for high performance C-IPSCs are summarized and the film fabrication process strategies for $CsPbBr_3$, $CsPbIBr_2$, $CsPbI_2Br$, and $CsPbI_3$ are systematically discussed, respectively. In addition, the prospects for future film fabrication processes for C-IPSCs are proposed.

Keywords: all-inorganic perovskite solar cells; thin film; film fabrication; high efficiency; stability

check for updates

Citation: Yang, H.; Wang, H.; Wang, K.; Liu, D.; Zhao, L.; Chen, D.; Zhu, W.; Zhang, J.; Zhang, C. Recent Progress of Film Fabrication Process for Carbon-Based All-Inorganic Perovskite Solar Cells. *Crystals* **2023**, *13*, 679. https://doi.org/10.3390/cryst13040679

Academic Editor: Sawanta S. Mali

Received: 20 March 2023
Revised: 4 April 2023
Accepted: 11 April 2023
Published: 14 April 2023

Copyright: © 2023 by the authors. Licensee MDPI, Basel, Switzerland. This article is an open access article distributed under the terms and conditions of the Creative Commons Attribution (CC BY) license (https://creativecommons.org/licenses/by/4.0/).

1. Introduction

Among the next generation of photovoltaic technologies, the remarkable perovskite solar cells (PSCs) were first reported in 2009 [1]. The initial power conversion efficiency (PCE) of PSCs is only about 3% but, due to their unique properties—high light absorption efficiency [2,3], tunable band gap [4,5], small exciton binding energy [6], high carrier mobility [7,8] etc.—they have rapidly gained widespread attention from the photovoltaic research community worldwide. The certificated PCE has surged to 25.7% [9]. With the fast growth of PCE and low-cost preparation process, PSCs are expected to be commercially available in coming years [10–12].

The general molecular formula of perovskite adopted in the photovoltaic field is ABX_3, whose crystal structure is shown in the inset of Figure 1a, where A is monovalent cation such as methylammonium ($CH_3NH_3^+$; MA^+) or formamidinium ($HC(NH_2)_2^+$; FA^+) or Cs^+, B is divalent metal such as Pb^{2+} or Sn^{2+}, and X is a monovalent halide anion such as Cl^- or Br^- or I^-. PSCs with PCE exceeding 22% are mostly made of organic-inorganic perovskite

film containing organic components (MA^+ or FA^+) [13–16]. Although organic-inorganic perovskite films have excellent photovoltaic properties, the inherent stability of the organic component [17–19], especially thermal stability [20,21], is very poor. For instance, $MAPbCl_3$ and $FAPbCl_3$ films decomposed to some extent under one of the standard test conditions ISOS−D−2 (85 °C) [22]. These disadvantages limit the scope of application of PSCs.

The most effective way to improve the long-term stability and thermal stability of PSCs is to completely replace the organic component of A in the ABX_3 with an inorganic component [23,24]. Since 2015, researchers have revealed that cesium lead halide PSCs have an excellent stability and the unencapsulated devices can operate continuously and stably for over 900 h at 100 °C [23,25–27]. In particular, hole-transporting materials (HTM)-free carbon-based cesium lead halide PSCs (C-IPSCs) exhibit two distinct advantages. Firstly, conventional small-molecule HTMs (spiro-OMeTAD: 2,2,7,7-tetrakis (N,N-di-p-methoxyphenylamine)-9, 90-spirobifluorene) and polymer HTMs (PTAA: poly(triarylamine)) in IPSCs require dopants, such as lithium bis (trifluoromethanesulfonyl) imide (LiTFSI) and tert-butylpyridine (tBP), which leads to the hydrophilicity of HTM layer, thus accelerating the decomposition of perovskite film and aggravating the long-term operational instability issues [28–30]. Secondly, precious metal electrodes such as Au used in IPSCs are expensive, and the HTMs are more than 10 times more expansive than Au electrodes [31,32]. By eliminating the HTM layers in the configuration of C-IPSCs and using low-cost carbon electrodes, C-IPSCs have the remarkable advantage of high stability and low cost. The main advantages of carbon electrodes are low cost, suitable work function with all-inorganic perovskite, simple process, and inertness to water and ions in perovskite. There are two major disadvantages of carbon electrodes. First, the adhesion between the carbon electrode and the perovskite is not dense enough, which easily leads to the recombination of carriers at the interface [33,34]. Second, the carbon electrode is less reflective of sunlight compared to the Ag/Au electrode, resulting in less secondary absorption of sunlight by the perovskite layer.

Up to date, C-IPSCs have shown high stability, while performance is still far below their Shockley-Queisser limit [35]. For instance, the top level PCE of $CsPbI_3$-based devices reported so far is about 15%, which is only 50% of the Shockley-Queisser limit [36–38]. In order to increase the progress of large-scale commercialization of C-IPSCs, it is necessary to overcome the obstacles, such as further enhancement of PCE of C-IPSCs, decreasing energy level difference at the interfaces for more efficient carrier transport, and improvement of phase stability of the all-inorganic perovskite films. The most effective way to solve these issues is to fabricate high-quality inorganic perovskite films. However, there are great differences in the optical properties, optoelectronic properties, and device performance of C-IPSCs obtained by methods such as one-step solution process, two−step solution process, vacuum process, and vapor-assisted process.

In this review, we first discuss the primary challenges associated with the high-quality films fabrication process for C-IPSCs. Due to the large differences in the optoelectronic properties, film formation mechanism, and stability of the inorganic films, we then discuss and summarize in detail the representative films fabrication processes for $CsPbBr_3$, $CsPbIBr_2$, $CsPbI_2Br$, and $CsPbI_3$ films of C-IPSCs. Finally, we provide our perspectives and an outlook of possible solutions for the film fabrication process for C-IPSCs.

2. Primary Challenges with Film Fabrication Process for C-IPSCs

2.1. Energy Level Mismatch

Because the unstable and expensive HTM is eliminated from the structure of C-IPSCs, the device has a configuration of glass/electron transport material (ETM)/perovskite/carbon, as shown in Figure 1a, where compact TiO_2 (c−TiO_2) and/or mesoporous TiO_2 (m−TiO_2) is typically used as ETM. The energy level diagram of $CsPbBr_3$, $CsPbIBr_2$, $CsPbI_2Br$, and $CsPbI_3$ C-IPSCs is shown in Figure 1b. The energy difference between the conduction band minimum (CBM) of TiO_2 layer and the all-inorganic perovskite film is so large that it tends to cause electrons to flow back to the interface of TiO_2/perovskite [39]. These electrons

can easily recombine with holes through deep level defects, thus reducing the PCE of the devices. It is obvious that there is energy level mismatch between the interfaces, which leads to carrier recombination and, thus, affects the performance of the devices [40–42].

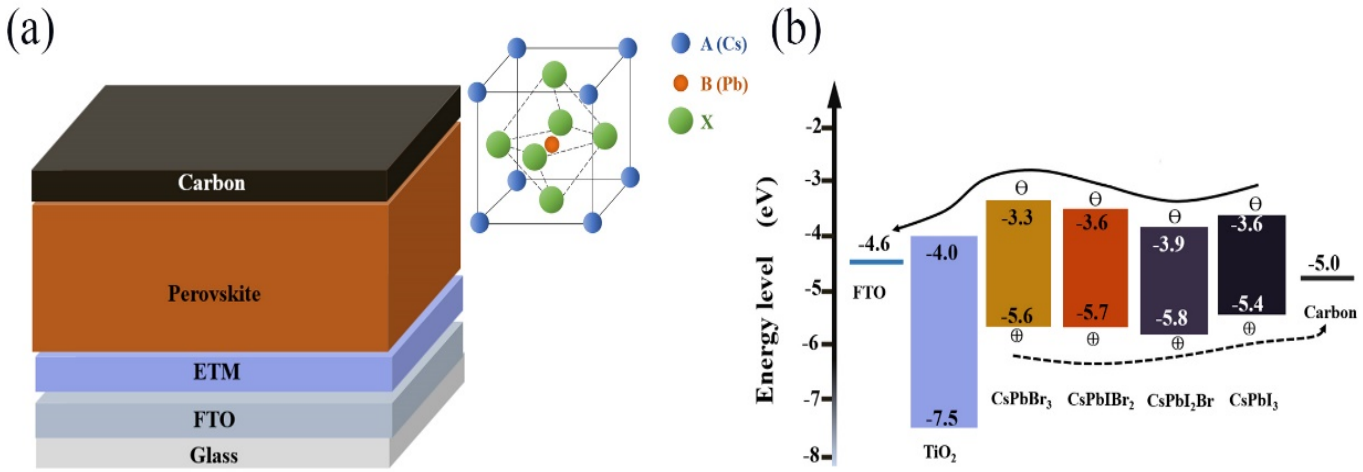


Figure 1. (**a**) The device configuration (inset: crystal structure of perovskite films) and (**b**) the energy level diagram of $CsPbBr_3$, $CsPbIBr_2$, $CsPbI_2Br$, and $CsPbI_3$ C-IPSCs. The band structures of FTO, TiO2, carbon, and perovskite films are referred to from the previous literature [25,42–44].

Certainly, the energy level alignment can be improved by interface engineering, such as modifying the ETM or the carbon electrode layers [41,45–48]. However, the more effective and convenient strategy is to achieve energy level alignment by optimizing the perovskite film fabrication process to enhance the performance of the devices while modifying the valence band maximum (VBM) or the conduction band minimum (CBM) of the inorganic films [49–51], which will be discussed in more detail in the later part of this review.

2.2. Phase Stability

The phase stability of perovskite films can be predicted by the Goldschmidt tolerance factor t and octahedral factor μ:

$$t = \frac{r_A + r_X}{\sqrt{2}(r_B + r_X)} \quad (1)$$

$$\mu = \frac{r_B}{r_X} \quad (2)$$

where r_A, r_B, and r_X are the ionic radii of A, B, and X in the perovskite formula ABX_3, respectively [52,53].

It is generally accepted that the stable black inorganic perovskite with photovoltaic properties can only be formed when $0.813 < t < 1.107$ and $0.442 < \mu < 0.895$ [53]. Due to the smaller ionic radius of Cs^+ (1.81 Å) compared to the organic ions MA^+ (2.70 Å) and FA^+ (2.79 Å), the t values for $CsPbBr_3$, $CsPbIBr_2$, $CsPbI_2Br$, and $CsPbI_3$ range from 0.814 ($CsPbBr_3$) to 0.81 ($CsPbI_3$) and the value μ ranges from 0.62 ($CsPbBr_3$) to 0.54 ($CsPbI_3$) [54,55]. It is the weakest phase stability for $CsPbI_3$ films (E_g: ~1.8 eV), which have a broader absorption spectrum and greater potential for higher efficiency. The stability of C-IPSCs is significantly better than that of organic-inorganic PSCs. However, stability remains a challenge for C-IPSCs, especially for CsPbI3 C-IPSCs. Here are some strategies that have been proposed to improve the stability of C-IPSCs:

Encapsulation: $CsPbI_3$ is sensitive to moisture, heat, and light, which can degrade the perovskite film and reduce the device stability. Encapsulating the device with suitable barrier layers, such as polymer, glass, or metal, can protect the device from environmental factors and improve its stability.

Interface engineering: Interfaces in C-IPSCs, such as those between the perovskite and the electron transport layer or carbon electrode, can also affect the device stability. The introduction of a suitable interlayer or interface modifier can improve the charge transfer and reduce interface recombination, leading to improved device stability [56,57].

Doping: Doping the perovskite film with suitable materials, such as metals or metal oxides, can improve the stability of the device by reducing the trap density and improving the charge transport properties [58–60].

Composition engineering: The composition of the perovskite film can also affect the stability of the device. Introducing suitable additives, such as dimethylammonium iodide [36] and CsI [61], can improve the crystal quality and reduce the defect density in the perovskite film, leading to improved device stability.

Passivation of defects: Defects in perovskite films can lead to charge carrier recombination and reduce the device stability. Passivation of these defects by using organic or inorganic materials, such as alkali hydroxides [45], N, N'-Dicyclohexylcarbodiimide (DCC) [62], or halogenoid ions [63], can improve the device stability.

Overall, the strategies mentioned above can be combined to achieve the best stability improvement results for C-IPSCs.

Therefore, the main consideration in film fabrication processes should be how to improve the stability.

2.3. Exceeding the Solubility Limit of Cs Salts

Since the device configuration of C-IPSCs and the all-inorganic perovskite components are significantly different from those of organic-inorganic hybrid halide PSCs, it is more complicated to regulate the fabrication process of inorganic perovskite films for C-IPSCs. How to exceed the solubility limit of Cs salts is very important in the film fabrication process.

Firstly, the trade−off between band gap and phase stability of perovskite films requires precise control of the halide composition regulation. However, the solubility limit of Cs salts, especially CsBr, in N,N-dimethylformamide (DMF) is very low, so a certain amount of dimethyl sulfoxide (DMSO) with higher polarity index should be mixed into the solvent to improve the solubility of CsBr [64,65]. However, the boiling point of DMSO (189 °C) is higher than that of DMF (153 °C), which will slow down the crystallization process of all-inorganic perovskite, resulting in a large number of pinholes in the films [66,67].

Secondly, due to the weak light reflectance ability of carbon-electrode-based IPSCs compared to metal Au/Ag-based IPSCs, the effective secondary absorption cannot be established [68–70]. To achieve more light absorption, it is necessary to fabricate thicker inorganic layers compared to metal electrode devices (~400 nm) [70,71]. For the above reasons, it is necessary to exceed the solubility limit by methods such as vapor deposition [72,73], precursor composition engineering [61,74], and post-annealing processing [75–77]. In particular, it is more important to exceed the solubility limit of Cs salts for large-scale industrial film fabrication processes, such as spray coating, inkjet-printing, etc. [78–80].

In addition to the above three main challenges, there are also some concerns in the film fabrication process of IPSCs: it was found that the self-trapped electrons (STEL) and holes (STH) in $PbCl_2$ and $PbBr_2$, which are one of the important components in the formation of all-inorganic perovskite, have an important influence on carrier recombination. Meanwhile, due to the different halogen-halogen distances in CsCl, CsBr, and CsI crystal structure, the temperature for STH migration onset is different, which has an important impact on the PV characteristics of C-IPSCs (as shown in Table 1) [81,82].

In addition, there is phase segregation upon illumination due to the kinetic mechanism of film formation [33,83], severe nonradiative recombination due to defects in the film [84,85], insufficient environmentally friendly solvents used in the solution methods [86,87], etc.

Table 1. A summary of the calculated STEL and STH for PbX_2 (X=Cl, Br, I) and the initial migration temperatures for the STH in CsX (X=Cl, Br, I).

Material	STEL	STH	Material	Halogen-Halogen Distance (Å)	Migration Temperatures (K)
$PbCl_2$	Pb_2^{3+}	Pb^{3+}	CsCl	4.123	202
$PbBr_2$	Pb_3^{5+}	Pb^{3+}	CsBr	4.286	122;130
PbI_2	None	None	CsI	4.567	60;85

The advantages and disadvantages of C-IPSCs with $CsPbBr_3$, $CsPbIBr_2$, $CsPbI_2Br$, and $CsPbI_3$ films are summarized in Table 2.

Table 2. A summary of the advantages and disadvantages of different C-IPSCs.

C-IPSCs	Advantages	Disadvantages
$CsPbBr_3$	1. Excellent stability in ambient air 2. All fabrication in ambient air	1. Large bandgap (~2.3 eV) 2. Difficult to control film formation 3. Low PCE
$CsPbIBr_2$	1. Good stability in ambient air 2. All fabrication in ambient air	1. Higher bandgap (~2.05 eV) 2. Energy level mismatch
$CsPbI_2Br$	1. Proper bandgap (~1.90 eV) 2. Good thermal stability	1. Humidity instability 2. Inferior phase stability
$CsPbI_3$	1. Most suitable bandgap (~1.73 eV) 2. Excellent light absorption performance 3. Highest efficiency achieved	1. Weakest phase stability 2. Worst thermal and moisture stability

More importantly, the film fabrication process for $CsPbBr_3$, $CsPbIBr_2$, $CsPbI_2Br$, and $CsPbI_3$ films of C-IPSCs has some different concerns. In the third part of this review, the film fabrication processes for $CsPbBr_3$, $CsPbIBr_2$, $CsPbI_2Br$, and $CsPbI_3$ films of C-IPSCs are discussed, respectively.

3. Strategies of Film Fabrication Process for C-IPSCs

3.1. $CsPbBr_3$

Due to the remarkable stability of $CsPbBr_3$ film, the C-IPSCs based on $CsPbBr_3$ were first proposed among all the C-IPSCs in 2016 [88]. It is difficult to achieve accurate stoichiometric ratios of precursors by the conventional one-step method because of the low solubility of CsBr in DMF or DMSO, so the two-step solution method and multi-step solution method are the mainstream strategies for $CsPbBr_3$ film fabrication process for C-IPSCs [89–93].

Jin et al. adopted the two-step solution; the first step is to prepare the $PbBr_2$ layer by the solution of 1.0 M $PbBr_2$ in DMF spin-coated on the substrate of $c-TiO_2$ and $m-TiO_2$, then drying at 80 °C for 30 min [88]. In the second step, the solution of 0.07 M CsBr in methanol was dipped onto the substrate for 10 min, and afterwards rinsed by isopropanol, dried in air, and heated to 250 °C for 5 min, resulting in $CsPbBr_2$ film. It is worth mentioning that the whole preparation process of C-IPSCs was accomplished in ambient air, which means lower fabrication costs. Through optimizing the thicknesses of $m-TiO_2$ and $PbBr_2$ layers, the best performance achieved a 6.7% PCE with an active area of 0.12 cm^2. Moreover, the unencapsulated cells showed no degradation in performance after 860 h under extreme conditions (100 °C, 90–95% relative humidity (RH)). The high stability and low cost of C-IPSCs aroused much attention, but the initial C-IPSCs had to be prepared on the complicated $c-TiO_2$ and $m-TiO_2$ substrate.

Yang et al. revised the two-step solution method by innovatively proposing the face-downing dipping process, by which the best performance cell with a PCE of 5.86% and higher open-circuit voltage (V_{OC}) of 1.34 V was prepared on the relatively simple $c-TiO_2$ substrate, on which it is more difficult to prepare homogeneous and pinhole-free $CsPbBr_3$

films (as shown in Figure 2a) [94]. In order to find out the optimal dipping parameters, the substrates were dipped face down in CsBr solution at 50 °C from 10 min to 60 min. As shown by the corresponding SEM images in Figure 2b, when the dipping time reached 40 min, the surface morphology of the $CsPbBr_3$ film is uniform and smooth, with the average grain sizes increasing to 860 nm. In addition, the PCEs of that device remained mostly unchanged in an ambient environment of 50–60% RH at 25 °C.

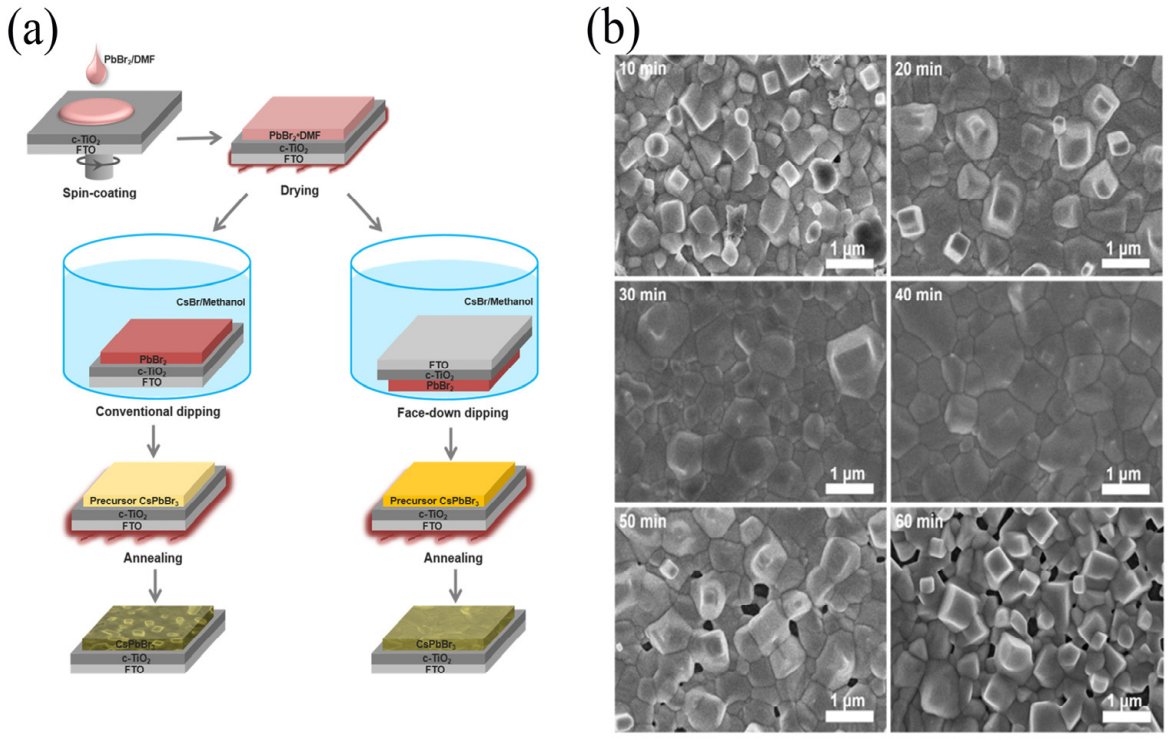


Figure 2. (**a**) Schematic fabrication for $CsPbBr_3$ films obtained by conventional process and face-down dipping process and (**b**) SEM images of CsPbBr3 perovskite films face-down dipped at 50 °C for 10 min, 20 min, 30 min, 40 min, 50 min, and 60 min, respectively. Reproduced with permission [94]. Copyright 2018, American Chemical Society Publications.

The formation of $CsPb_2Br_5$ or Cs_4PbBr_6 due to incomplete reactions is the main reason for the relatively low PCE for $CsPbBr_3$ C-IPSCs [95–97]. Therefore, how to obtain a high purity $CsPbBr_3$ phase is the main concern in the film preparation process. Consequently, a diversity of multi-steps of spin-coating CsBr solution had been developed for accurate control of the crystallization process of $CsPbBr_3$ to avoid formation of mixed phases. Wu et al. fabricate pinhole-free and phase-pure $CsPbBr_3$ film through an innovative triple-step solution method, as shown in Figure 3a [93]. The highlight of this method is the use of the green bi-solvent of water (the high polarity index) and ethylene glycol monomethyl ether (EGME with high viscosity) to dissolve CsBr. Through twice spin-coating CsBr solution, the reaction kinetics were balanced and Ostwald ripening was achieved. Compared to adopting methanol as the solvent for CsBr, adopting water/EGME bi-solvent system can form a homogenous $CsPbBr_3$ film without any phase separation, as illustrated in Figure 3b. The optimal device is a PCE of 9.55% with a fill factor (FF) of 84.49%, a short-circuit photocurrent density (J_{SC}) of 7.18 mA/cm^3, an open-circuit photovoltage (V_{OC}) of 1.5 V, and a PCE of the unencapsulated device was maintained at 86.8% of its initial value after 34 days in an open-air environment.

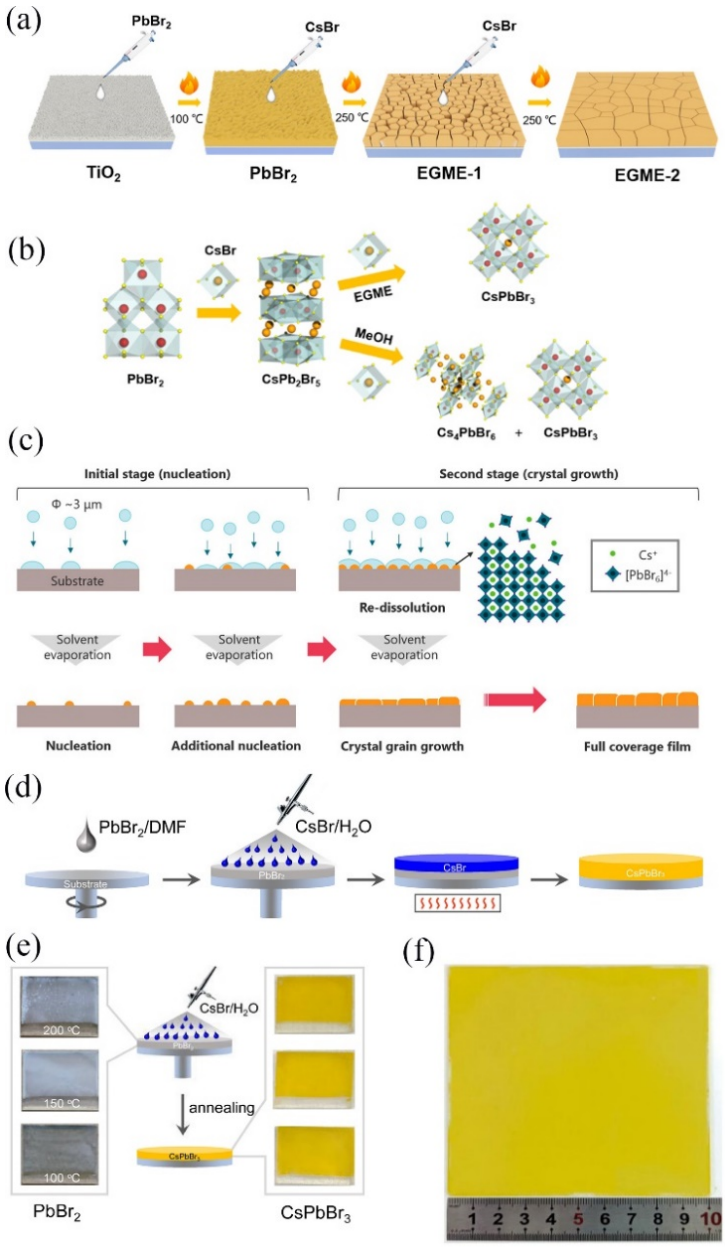


Figure 3. (**a**) Schematic diagram of the triple-step solution method for the fabrication process of $CsPbBr_3$ films and (**b**) schematic illustration of the phase conversion process of Cs-Pb-Br films through various bi-solvent solutions. Reproduced with permission [93]. Copyright 2022, Elsevier Inc. Publications. (**c**) Schematic diagram of the mist deposition method for full-coverage $CsPbBr_3$ [79]. Copyright 2020, American Chemical Society Publications. (**d**) Schematic illustration of water-based spray-assisted method for scalable $CsPbBr_3$ film. (**e**) Photographs of $CsPbBr_3$ films by spray-assisted method with the thermal treatment temperature for $PbBr_2$ at 100 °C, 150 °C, and 200 °C. (**f**) Photograph of $CsPbBr_3$ film with the area up to 10 × 10 cm^2 [80]. Copyright 2021, Elsevier Inc. Publications.

In addition to the spin-coating methods, the fabrication processes of $CsPbBr_3$ films suitable for large-scale production are of great interest to the industry, such as spray coating [80], misting treatment [79], thermal evaporation process [98,99], etc. Hirato et al. adopted misting treatment in which the small and uniform mist particles of the precursor solution were first generated by a 2.4 MHz ultrasonic vibration [79]. Then, these mist particles were deposited on the preheated substrate through two stages: initial stage and crystal growth, as shown in Figure 3c. Finally, the area of the uniform $CsPbBr_3$ film obtained by this method can be up to 2.5 × 2.5 cm^2. However, duo to the limitation of electrode

area, the final area of the devices is only 0.08–0.10 cm^2. Our team proposed a generic spray-assisted film process, which is suitable for large-scale production for IPSCs [80]. The film preparation process is shown in Figure 3d. First, $PbBr_2$ solution was spin-coated onto the substrate. Through the annealing process, the water-based CsBr solution was sprayed onto the surface of the $PbBr_2$ film using a commercial airbrush. The PCE of the optimal device with an area of up to 1 cm^2 was 8.21%, which is a record efficiency for the large-area $CsPbBr_3$ cells reported to date. In addition, this spray-assisted method has a high degree of process compatibility with different morphologies of $PbBr_2$ films. The morphologies of $CsPbBr_3$ films were almost identical with the annealing temperature of $PbBr_2$ films at 100 °C, 150 °C, and 200 °C (Figure 3e). At the same time, this method also shows generic applicability for the preparation of $CsPbIBr_2$ films, $CsPbI_2Br$ films, and $CsPbCl_3$ films. The area of $CsPbBr_3$ films can be scaled up to 10 × 10 cm^2 by adopting this method (Figure 3f), so the large-scale film fabrication processes for C-IPSCs have great potential for further research.

The stability of $CsPbBr_3$ C-IPSCs is excellent but their PCE is currently mostly below 10%. Therefore, further improvement of the crystalline quality, degree of coverage, grain size, and the film thickness of the $CsPbBr_3$ films is a major concern in future film fabrication processes.

3.2. $CsPbIBr_2$

As $CsPbIBr_2$ (E_g: ~2.1 eV) has a narrower band gap compared to $CsPbBr_3$ (E_g: ~2.3 eV), the C-IPSCs based on $CsPbIBr_2$ have the potential to achieve higher PCE. In addition, $CsPbIBr_2$ shows excellent stability in ambient air, even at high temperature [100–102]. Therefore, the C-IPSCs based on $CsPbIBr_2$ films can achieve a balance between efficiency and stability.

$CsPbIBr_2$ films can be deposited by solution [103–105], dual-source thermal evaporation [106], vapor-assisted [49,107], and spray-assisted methods [107]. Since the solubility of CsI in DMSO can reach 1M, the convenient one-step spin-coating solution by dissolving CsI and $PbBr_2$ into DMSO (~1.0 M) is the mainstream film fabrication process for $CsPbIBr_2$. However, in the process of crystallization dynamics of the one-step spin-coating solution for $CsPbIBr_2$ films, the weaker volatility of DMSO and the formation of CsI-$PbBr_2$-DMSO complexes during the spin-coating would introduce ionic vacancy into the $CsPbIBr_2$ films, which would form nonradiative recombination centers, resulting in poor device performance [50,75,108]. Therefore, the methods of intermolecular exchange [50,105], precursor solution additive engineering [51,75], pretreatment, and post-treatment [75] have been proposed to improve crystallization quality in the one-step solution $CsPbIBr_2$ film fabrication process.

Our team first proposed a facile intermolecular exchange approach for $CsPbIBr_2$ film fabrication [50]. The most essential step of this method is the spin-coating of an optimized concentration of CsI solution onto the $CsPbIBr_2$ precursor films to promote the crystallization of $CsPbIBr_2$ films. Finally, the pure-phase $CsPbIBr_2$ films with uniform morphology and a pinhole-free structure were obtained by annealing at 280 °C for 10 min. Since CsI have a stronger affinity for PbBr than DMSO, the intermolecular exchange took place between CsI and DMSO molecules to facilitate the formation of high-quality $CsPbIBr_2$ films (as shown in Figure 4a).

From the SEM images in Figure 4b,c, the film obtained by intermolecular exchange is fully covered with larger grain size, while the film obtained by conventional one-step solution has obvious voids and the grain size is small. In particular, as shown in Figure 4d,e, the CBM, the VBM, and the work function of the $CsPbIBr_2$ film are adjusted by intermolecular exchange so that the energy level mismatch of the devices is improved, which can suppress carrier recombination and increase the V_{OC} to 1.245 V. The champion PCE has reached 9.16% with excellent long-term stability.

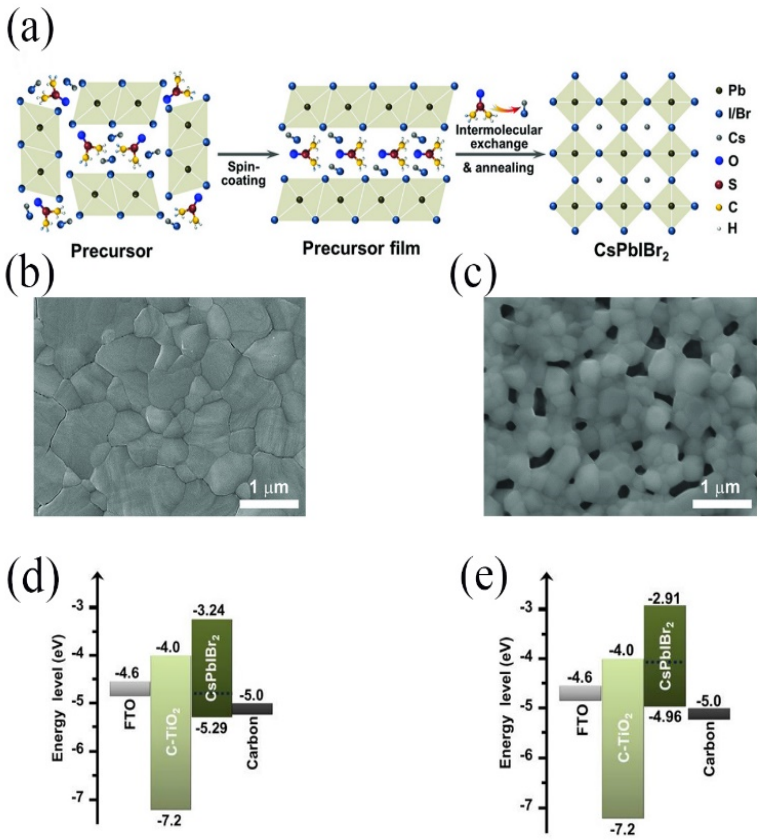


Figure 4. (**a**) Illustration of intermolecular exchange approach for $CsPbIBr_2$ film fabrication. SEM images of $CsPbIBr_2$ films obtained by (**b**) intermolecular exchange and (**c**) conventional one-step solution. (**d**) Energy level diagrams of $CsPbIBr_2$ films fabricated by intermolecular exchange and (**e**) conventional route. Reproduced with permission [50]. Copyright 2018, Wiley-VCH Publications.

Optimizing the substrate preheating and post-annealing temperature during the film fabrication process is also an effective approach to obtain high-quality $CsPbIBr_2$ films for fast removal of DMSO from precursor films. Wang et al. optimized the substrate preheating temperature and post-annealing temperature to 70 °C and 200 °C, respectively [75]. It can be clearly observed in Figure 5a–d that, when the substrate preheating reaches 70 °C, the $CsPbIBr_2$ film shows compact and uniform morphology with the largest grain size. The X-ray diffraction (XRD) peaks of the α-phase $CsPbIBr_2$ films are strongest when the temperature of post-annealing is 200 °C, which indicates higher crystalline quality (as shown in Figure 5e). As shown in Figure 5f, the peaks of the steady-state photoluminescence (PL) spectra for all $CsPbIBr_2$ films are centered at 595 nm, which is due to the radiation recombination of the $CsPbIBr_2$ films. In addition, PL peak corresponding to this temperature means that the $CsPbIBr_2$ film has the least defects.

To reduce the nonradiative recombination centers in $CsPbIBr_2$ films, doping with anions and/or cations in the film fabrication process is also an effective method. Guo et al. further improved the devices' performance by doping the precursor solution with multi-source cations/anions [51]. The $CsPbIBr_2$ film fabrication process is schematically shown in Figure 6a. In the first step, RbI (0.5%) was added to the precursor solution, followed by intermolecular exchange between the spin-coated CsAc solution and the $CsPbIBr_2$ precursor film. The introduction of Ac^- reduces the anion vacancy defects in the $CsPbIBr_2$ film to decrease the work function of the film, which increases the V_{OC} of the device (as shown in Figure 6b). In addition, the doping of Rb^+ can improve the crystalline quality of the $CsPbIBr_2$ film. As a result, the optimum PCE of $CsPbIBr_2$ C-IPSC up to 10.78% with V_{OC} of 1.37 V.

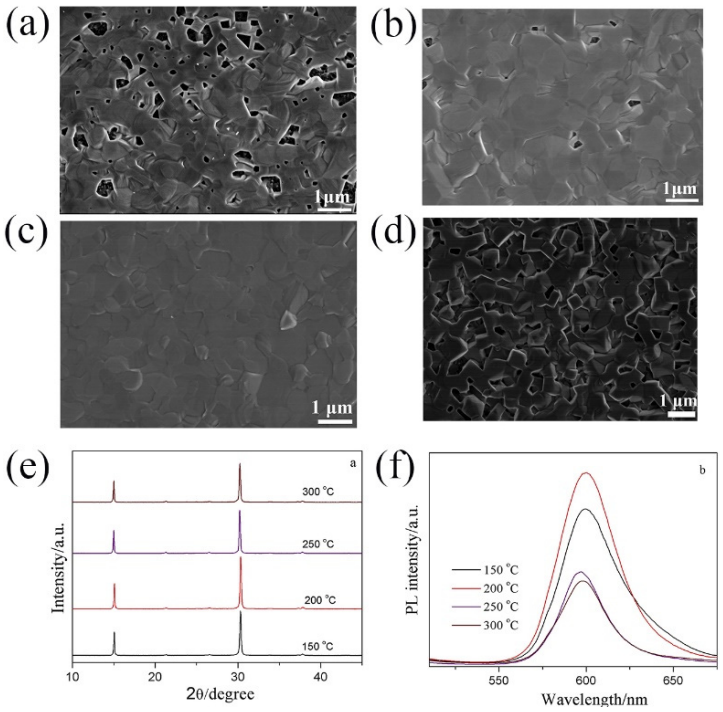


Figure 5. SEM images of $CsPbIBr_2$ perovskite films obtained at the substrate preheating temperatures of (**a**) 30 °C, (**b**) 50 °C, (**c**) 70 °C, and (**d**) 90 °C. (**e**) XRD patterns and (**f**) PL spectra of $CsPbIBr_2$ perovskite films formed at different preheating temperatures. Reproduced with permission [75]. Copyright 2020, Elsevier Inc. Publications.

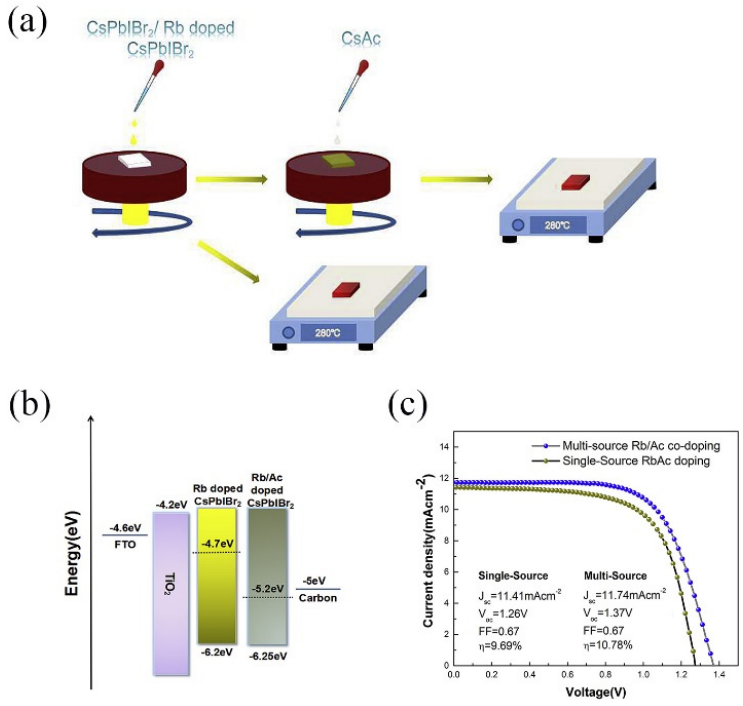


Figure 6. (**a**) Schematic illustration of fabrication of $CsPbIBr_2$ film by doping the precursor solution with multi-source cation/anion. (**b**) Energy-level diagram of $CsPbIBr_2$ C-IPSCs with Rb and Rb/Ac doped. (**c**) J–V curves of $CsPbIBr_2$ C-IPSCs with single-source and multi-source Rb/Ac doped. Reproduced with permission [51]. Copyright 2021, Elsevier Inc Publications.

The ionic vacancy in $CsPbIBr_2$ films resulting from the lower volatility of DMSO can also be improved by light-assisted [109], flux-mediated [110], and residual $CsPbIBr_2$-

derived species from the recycling substrates [111]. By these methods, the energy level mismatch of $CsPbIBr_2$ C-IPSC can also be improved. Recently, Luo et al. adopted solvent engineering by adding low boiling point methanol to DMSO, which effectively improved the crystallinity of the $CsPbIBr_2$ film [105]. In this way, the champion PCE of the devices with spiro-OMeTAD as HTM has exceeded 11%. In the future, this preparation of $CsPbIBr_2$ film is expected to be applied to C-IPSC.

3.3. $CsPbI_2Br$

$CsPbI_2Br$ has the more suitable band gap compared to $CsPbIBr_2$ and $CsPbBr_3$, which has the potential for higher PCEs. However, as the iodine component increases, the Goldschmidt tolerance factor t is close to 0.813, which means that the $CsPbI_2Br$ film is more easily transformed into the unfavorable perovskite yellow δ-phase at room temperature [112,113]. Therefore, it is important to consider how to improve the photovoltaic performance of the devices, as well as the stability of the phase stability of the $CsPbI_2Br$ film under ambient conditions during the film fabrication process.

Currently, $CsPbI_2Br$ films can be prepared by vacuum evaporation [114], spray-coating [115], and solution spin-coating [42,61,116,117]. Considering the relatively high solubility of CsI, PbI_2, and $PbBr_2$ in DMF or DMSO, either the one-step solution process or the two-step solution process can be adopted to bring more flexibility to the fabrication of $CsPbI_2Br$ films. The one-step solution process is convenient and easy to prepare for $CsPbI_2Br$ films but it has some limitations in controlling the film thickness and morphology compared with the two-step solution process. Therefore, there are advantages and disadvantages to the different film processes.

Dong et al. adopted the one-step solution processes and dropped chlorobenzene (CB) or ethyl acetate (EA) as antisolvent onto the precursor film at 30 s from the beginning of spin-coating (as illustrated in Figure 7a) [86]. The introduction of the antisolvent for $CsPbI_2Br$ films has a similar effect as for organic-inorganic perovskite films [118], which accelerated the crystallization, resulting in a more homogeneous and smoother surface morphology. More importantly, they had revealed through in-depth research that the devices prepared by adopting eco-friendly EA as the antisolvent achieved a champion PCE of 10.0%. The additive engineering of the precursor solution in the one-step process can also effectively improve the quality and stability of $CsPbI_2Br$ films [42,119,120]. Meng et al. added excess CsI to the precursor solution, in which the (110) plane of CsI and the (200) plane of $CsPbI_2Br$ could be able to match well to form spinodal decomposition (as shown in Figure 7b) [61]. The co-crystallization between CsI and $CsPbI_2Br$ not only formed a dense surface morphology and a phase-pure cubic $CsPbI_2Br$ perovskite structure, but also improved the energy band matching to reduce the carrier recombination due to the excess CsI (Figure 7c–e). The champion C-IPSC-based $CsPbI_2Br$ achieved a PCE of 10.13% and very good long-term stability at 80 °C for 200 h with only 10% loss of PCE.

Although the one-step solution process is relatively convenient, the performance of the devices is generally low, only about 10%. The two-step solution process can precisely control the growth process of $CsPbI_2Br$ films, which has great potential for fabricating higher performance C-IPSC-based $CsPbI_2Br$. Our team adopted the two-step solution process to form a precursor film composed of Cs-Pb-Br complex, which was finally transformed into $CsPbI_2Br$ films containing CsBr by annealing (as shown in Figure 8a) [121]. In the second spin-coating process, water was innovatively used as the solvent for CsI, and the dose of CsI/H_2O was optimized to 105 μL, which resulted in $CsPbI_2Br$ films with high crystallinity and large grain sizes were achieved, as indicated by the SEM images and XRD patters (Figure 8b–e). After optimized annealing, the Ruddlesden-Popper perovskite intermediate-phase film composed of Cs-Pb-Br complex was converted into $CsPbI_2Br$ grains and CsBr species by the spinodal decomposition reaction, and the mechanism of film formation is shown in Figure 8f. The atomic force microscope (AFM) and Kelvin probe force microscope images (Figure 8g,h) of the final $CsPbI_2Br$ film indicated that the surface was relatively uniform and, especially, the cross-sectional SEM image (Figure 8i) of the device showed

that the thickness of the $CsPbI_2Br$ film reached an excellent 460 nm. As a result, the PCE of the device reached 15.24%, which is the highest value of C-IPSC-based $CsPbI_2Br$. It is worth mentioning that the whole fabrication process is completed in ambient air, while the devices have excellent stability in ambient air with RH of 60–70%.

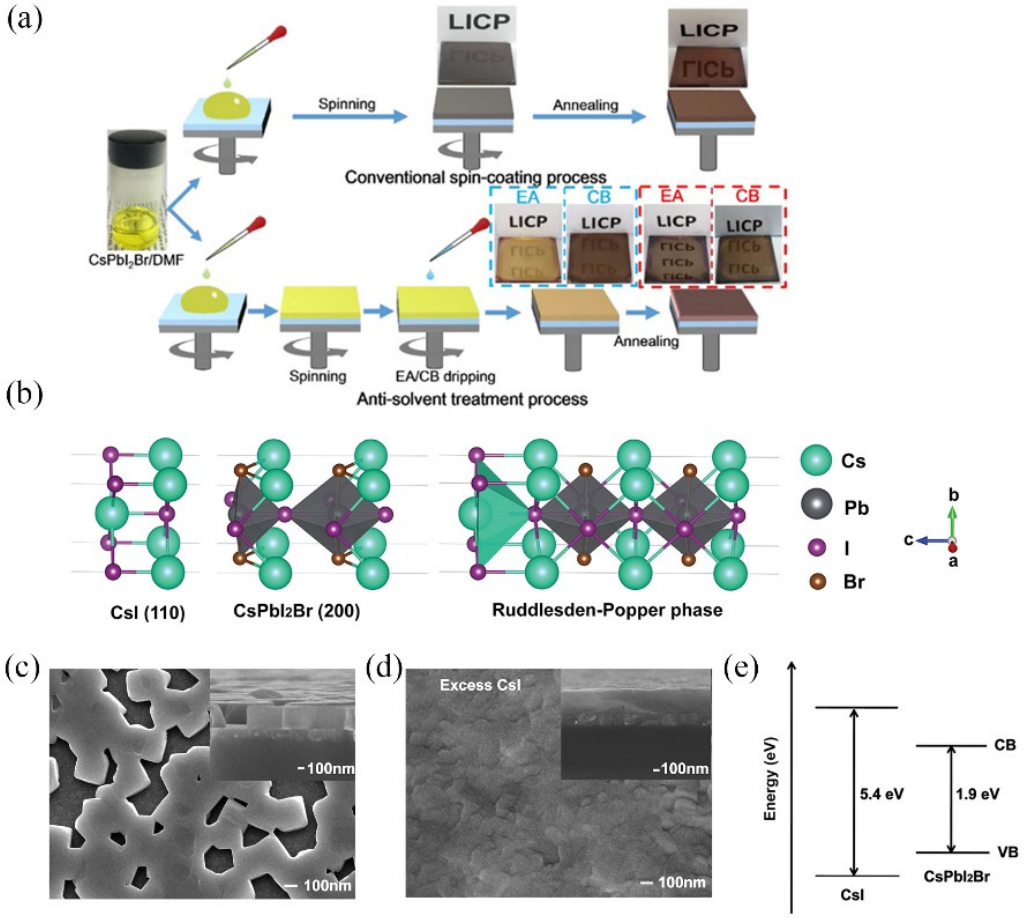


Figure 7. (**a**) Schematic illustration of conventional one-step solution processes and antisolvent treatment processes (with EA and CB as antisolvents) for fabricating $CsPbI_2Br$ C-IPSCs. Reproduced with permission [86]. Copyright 2018, Wiley−VCH Publications. (**b**) Schematic illustration of the crystal structures of the CsI phase, $CsPbI_2Br$ perovskite phase, and Ruddlesden-Popper phase. SEM image of the $CsPbI_2Br$ films without CsI (**c**) and excess CsI (**d**) and (**e**) energy level alignment of CsI and $CsPbI_2Br$. Reproduced with permission [61]. Copyright 2019, American Chemical Society Publications.

3.4. $CsPbI_3$

Among all-inorganic C-IPSCs, the C-IPSCs based on $CsPbI_3$ have the greatest potential to achieve high PCEs due to the smallest bandgap of $CsPbI_3$ (~1.73 eV) [122,123]. However, $CsPbI_3$ films are also the worst in terms of thermal and moisture stability and easily transform into yellow δ-$CsPbI_3$ at room temperature [124–126]. To improve the phase stability of $CsPbI_3$ films, ion doping and additive engineering [60,127,128] are usually employed in the fabrication process of $CsPbI_3$ films for C-IPSCs.

The addition of HI into the precursor solution was first proposed by Snaith et al. in 2015 [124], which significantly improved the phase stability of $CsPbI_3$ at room temperature, with a PCE up to 2.9% based on the regular architecture. Chen et al. used HI for mixing and reaction with PbI_2 to derive $HPbI_3$. Subsequently, $HPbI_3$ and CsI were dissolved in DMF to form a precursor solution (referred to as $HPbI_3$ precursor) [127]. The introduction of the HI additive resulted in the lattice expansion, which led to tensile lattice strain and,

thus, improved film stability. As shown in Figure 9a, the fabrication of $CsPbI_3$ films using the $HPbI_3$ precursor can employ a lower temperature (200 °C) compared to the adopted precursor conventional solution (PbI_2 and CsI in DMF labelled as PbI_2-precursor), and the phase stability of $CsPbI_3$ films is significantly improved, as the films can retain their black color for several days in dry air. The SEM images showed that the coverage and density of the $CsPbI_3$ film obtained from the $HPbI_3$ precursor were obviously better than those of the film obtained from the PbI_2 precursor (Figure 9b,c). The $CsPbI_3$-C-IPSCs-based $HPbI_3$ precursor achieved a champion PCE of 9.5% and can remain unencapsulated in dry air conditions for 3000 h with only 10% loss of PCE.

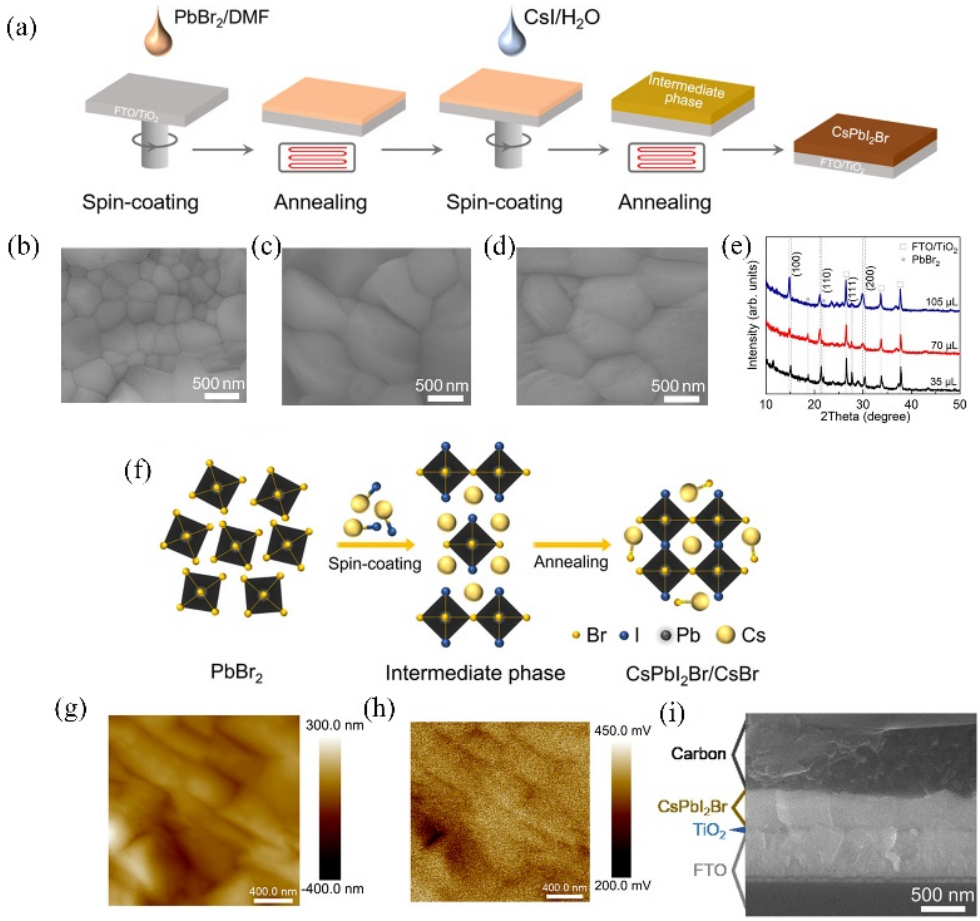


Figure 8. (**a**) Schematic illustration involving the intermediate-phase-assisted two-step solution process. SEM images of $CsPbI_2Br$ films prepared with (**b**) 35 μL, (**c**) 70 μL, and (**d**) 105 μL CsI/H_2O. (**e**) XRD patterns of $CsPbI_2Br$ films prepared with 35 μL, 70 μL, and 105 μL CsI/H_2O. (**f**) Formation mechanism of $CsPbI_2Br$ film with excess CsBr by intermediate-phase-assisted two-step solution process. (**g**) AFM and (**h**) Kelvin probe force microscope images of $CsPbI_2Br$ films fabricated by intermediate phase-assisted sequential process. (**i**) Cross-sectional SEM image of the resulting C-IPSC-based $CsPbI_2Br$ films. Reproduced with permission [121]. Copyright 2022, Wiley-VCH Publications.

In recent years, Chen and his colleagues adopted the $HPbI_3$ precursor, in which Na doping has also been applied [60]. The smoothness and grain size of the films were further enhanced by Na doping, as shown in Figure 9d,e. At the same time, the Fermi level of the films was raised for energy-level matching, which increased the V_{OC} of the device from 0.77 V to 0.92 V (as shown in Figure 9f).

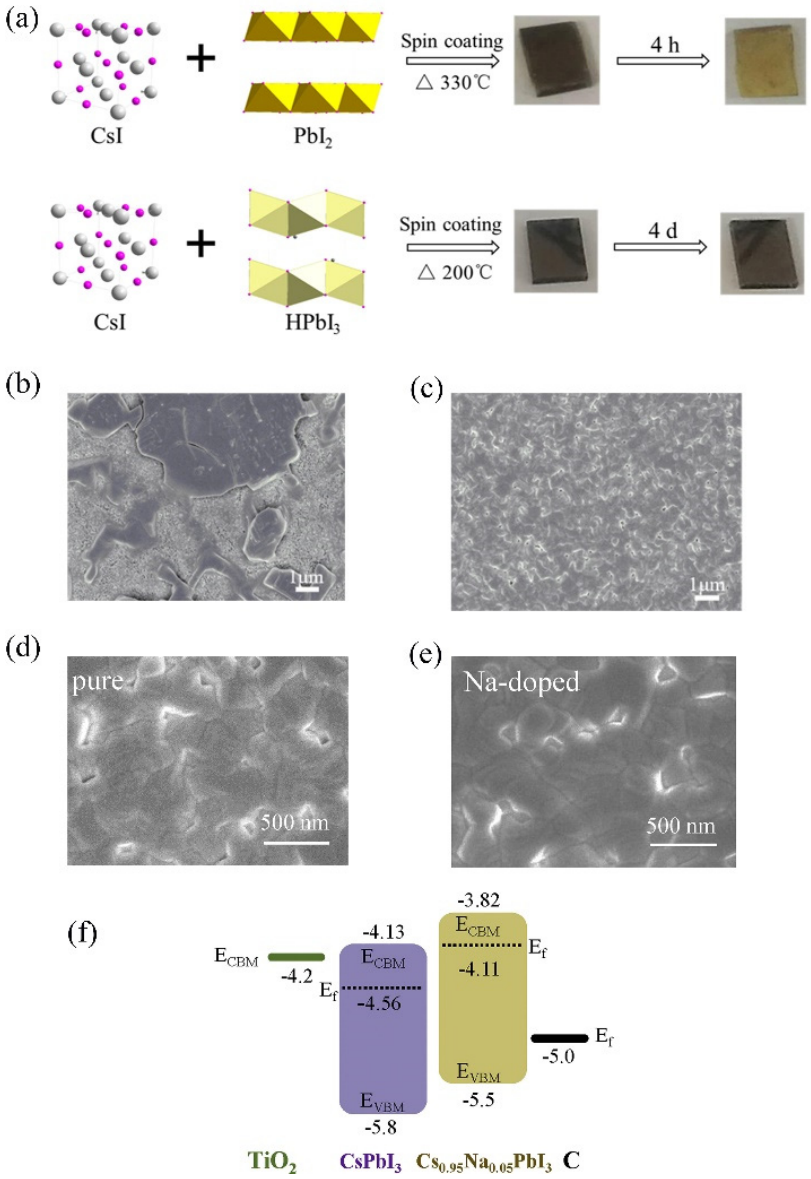


Figure 9. (**a**) Formation mechanism and phase structure of the CsPbI3 films from PbI2 precursor and HPbI3 precursor. SEM images of CsPbI2Br films prepared with (**b**) PbI2 precursor and (**c**) PbI2 precursor. Reproduced with permission [127]. Copyright 2018, American Chemical Society Publications. SEM images of CsPbI2Br films prepared without (**d**) and with (**e**) Na doping. (**f**) Energy-level diagrams of CsPbI3 C-IPSCs prepared without and with Na doping. Reproduced with permission [60]. Copyright 2019, Elsevier Inc. Publications.

More recently, Chen et al. innovatively incorporated ammonium halide as an additive into the precursor solution and promoted the crystallization of $CsPbI_3$ films by extracting ammonium halide by solvent (EAH-S), as illustrated in Figure 10a [128]. The film formation mechanism of perovskite phases of $CsPbI_3$ (p-$CsPbI_3$) was demonstrated in Figure 10b. Due to the introduction of ammonium halides, which tended to occupy the position of PbI_2 in transitive compounds, the formation of δ-phase of $CsPbI_3$ was inhibited. After immersion in a solvent with moderate polarity, p-$CsPbI_3$ nuclei were generated at the films' surface, followed by the formation of large p-$CsPbI_3$ grains. In combination with the extraction of ammonium halide by heating (EAH−H&S), high-quality p-$CsPbI_3$ films with PbI_2 passivator were achieved, resulting in a champion PCE of $CsPbI_3$ C-IPSCs of 15.35% and built-in potentials (V_{bi}) increasing up to 1.33 V (Figure 10c,d).

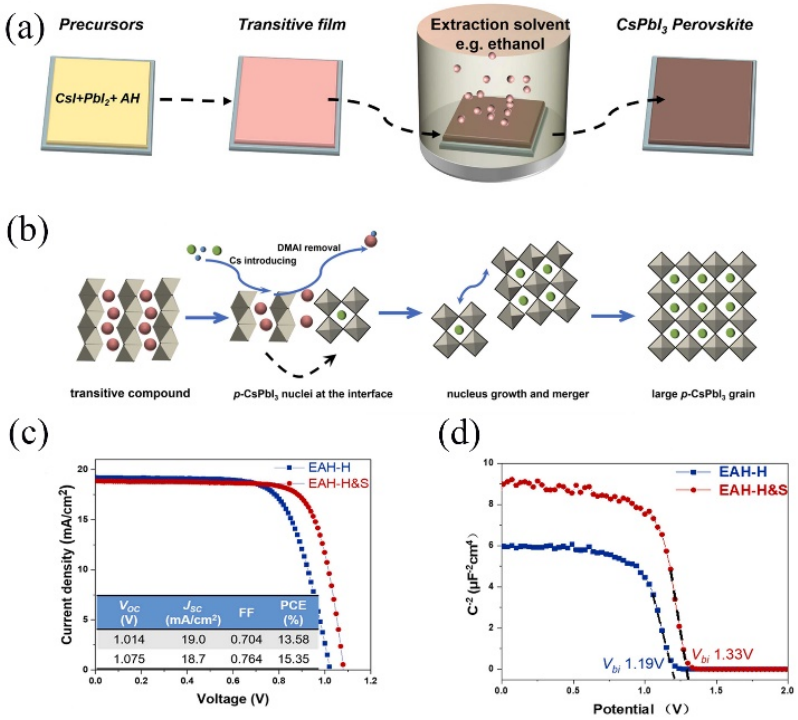


Figure 10. (**a**) Schematic illustration of EAH-S process. (**b**) Formation mechanism of CsPbI3 (p-CsPbI3) by EAH−S process. (**c**) J–V curves of $CsPbIBr_2$ C-IPSCs by EAH−H&S and EAH−H. (**d**) Mott-Schottky analysis plots at 10 kHz for $CsPbIBr_2$ films EAH−H&S and EAH−H. Reproduced with permission [128]. Copyright 2022, Elsevier Inc Publications.

There are other approaches to fabrication of $CsPbI_3$ films that are stable in dry air [129,130]. However, the poor stability in humid air is the main challenge for C-IPSCs based on $CsPbI_3$. Recently, Yang et al. found that laser irradiation accelerated the phase transition of $CsPbI_3$ under ambient moisture compared to without moisture. Therefore, the instability of $CsPbI_3$ under ambient moisture may be due to the interaction of defects, surface vacancies, and moisture [131]. Therefore, the effective reduction in defects in the $CsPbI_3$ films is essential for the film fabrication of high stable C-IPSCs based on $CsPbI_3$.

4. Conclusions

Carbon-based all-inorganic perovskite solar cells have the significant advantage of low cost and high stability in the field of photovoltaics. In recent years, the performance of C-IPSCs has been greatly improved through composition engineering, interface engineering, and, in particular, optimization of the film fabrication process. In this review, we have categorically summarized the recent progress of the film fabrication process for C-IPSCs.

C-IPSCs are promising for photovoltaic applications due to their high PCE and stability. However, there are still several challenges that need to be overcome for their commercialization:

Toxicity: Lead is a toxic material, and its use in C-IPSCs raises concerns about environmental and health impacts. Although there are efforts to reduce or eliminate lead content in perovskites, current lead−free alternatives often suffer from lower PCE or stability. This creates a challenge for C-IPSCs to be used in commercial applications due to environmental and health regulations.

Scalability: The scalability of the perovskite solar cell manufacturing process is another challenge. The C-IPSCs deposition process, which is often conducted using solution-based methods, can be difficult to scale up to large-area and high-throughput production. Moreover, the uniformity and reproducibility of the perovskite film are still challenges that need to be addressed for commercialization.

Lifetime: The lifetime of perovskite solar cells is still a challenge for commercialization. C-IPSCs have shown rapid degradation in accelerated aging tests, and the long-term stability and durability of these devices are still unknown.

In addition, a promising commercialization direction for all-inorganic perovskite films is to form two- or four-terminal tandem solar cells with silicon or organic solar cells to obtain wider absorption spectra under sunlight [54,132]. The technology of the fabrication process for all-inorganic thin films compatible with tandem devices is worthy of further research. Finally, the kinetic mechanism of film formation and the phase transition mechanism need to be further investigated.

In summary, IPSCs have shown great potential for photovoltaic applications but there are still challenges to overcome for commercialization, such as toxicity, scalability, lifetime, and the kinetic mechanism of film formation. These challenges need to be addressed through further research and development to make IPSCs a competitive alternative to traditional silicon solar cells.

Author Contributions: H.Y. and H.W. contributed equally to this work; H.Y., H.W., K.W., D.L. and L.Z. collected and summarized the literature; H.Y. wrote the manuscript; J.Z., W.Z., D.C. and C.Z. revised the manuscript. All authors have read and agreed to the published version of the manuscript.

Funding: This research was funded by Department of education project of Shaanxi province (Grant No. 20JS006), Department of Science and Technology Industrial Research Project, Shaanxi province, China (Grant No. 2016GY-226).

Institutional Review Board Statement: Not applicable.

Informed Consent Statement: Not applicable.

Data Availability Statement: The data presented in this study are openly available.

Conflicts of Interest: The authors declare no conflict of interest.

References

1. Kojima, A.; Teshima, K.; Shirai, Y.; Miyasaka, T. Organometal Halide Perovskites as Visible-Light Sensitizers for Photovoltaic Cells. *J. Am. Chem. Soc.* **2009**, *131*, 6050–6051. [CrossRef] [PubMed]
2. Green, M.A.; Ho−Baillie, A.; Snaith, H.J. The emergence of perovskite solar cells. *Nat. Photon.* **2014**, *8*, 506–514. [CrossRef]
3. Maes, J.; Balcaen, L.; Drijvers, E.; Zhao, Q.; De Roo, J.; Vantomme, A.; Vanhaecke, F.; Geiregat, P.; Hens, Z. Light Absorption Coefficient of CsPbBr3 Perovskite Nanocrystals. *J. Phys. Chem. Lett.* **2018**, *9*, 3093–3097. [CrossRef] [PubMed]
4. Weidman, M.C.; Seitz, M.; Stranks, S.D.; Tisdale, W.A. Highly Tunable Colloidal Perovskite Nanoplatelets through Variable Cation, Metal, and Halide Composition. *ACS Nano* **2016**, *10*, 7830–7839. [CrossRef]
5. Leng, K.; Abdelwahab, I.; Verzhbitskiy, I.; Telychko, M.; Chu, L.; Fu, W.; Chi, X.; Guo, N.; Chen, Z.; Chen, Z.; et al. Molecularly thin two-dimensional hybrid perovskites with tunable optoelectronic properties due to reversible surface relaxation. *Nat. Mater.* **2018**, *17*, 908–914. [CrossRef]
6. Yang, Y.; Yang, M.; Li, Z.; Crisp, R.; Zhu, K.; Beard, M.C. Comparison of Recombination Dynamics in CH3NH3PbBr3 and CH3NH3PbI3 Perovskite Films: Influence of Exciton Binding Energy. *J. Phys. Chem. Lett.* **2015**, *6*, 4688–4692. [CrossRef]
7. Leijtens, T.; Stranks, S.D.; Eperon, G.E.; Lindblad, R.; Johansson, E.M.J.; McPherson, I.J.; Rensmo, H.; Ball, J.M.; Lee, M.M.; Snaith, H.J. Electronic Properties of Meso−Superstructured and Planar Organometal Halide Perovskite Films: Charge Trapping, Photodoping, and Carrier Mobility. *ACS Nano* **2014**, *8*, 7147–7155. [CrossRef]
8. Oga, H.; Saeki, A.; Ogomi, Y.; Hayase, S.; Seki, S. Improved Understanding of the Electronic and Energetic Landscapes of Perovskite Solar Cells: High Local Charge Carrier Mobility, Reduced Recombination, and Extremely Shallow Traps. *J. Am. Chem. Soc.* **2014**, *136*, 13818–13825. [CrossRef]
9. Best Research-Cell Efficiency Chart. Available online: https://www.nrel.gov/pv/cell-efficiency.html (accessed on 5 February 2023).
10. Chen, J.; Park, N.-G. Materials and Methods for Interface Engineering toward Stable and Efficient Perovskite Solar Cells. *ACS Energy Lett.* **2020**, *5*, 2742–2786. [CrossRef]
11. Brown, A.A.M.; Damodaran, B.; Jiang, L.; Tey, J.N.; Pu, S.H.; Mathews, N.; Mhaisalkar, S.G. Lead Halide Perovskite Nanocrystals: Room Temperature Syntheses toward Commercial Viability. *Adv. Energy Mater.* **2020**, *10*, 2001349. [CrossRef]
12. Li, H.; Zhang, W. Perovskite Tandem Solar Cells: From Fundamentals to Commercial Deployment. *Chem. Rev.* **2020**, *120*, 9835–9950. [CrossRef]
13. Zheng, Z.; Li, F.; Gong, J.; Ma, Y.; Gu, J.; Liu, X.; Chen, S.; Liu, M. Pre-buried Additive for Cross−Layer Modification in Flexible Perovskite Solar Cells with Efficiency Exceeding 22%. *Adv. Mater.* **2022**, *34*, 2109879. [CrossRef]

14. Ru, P.; Bi, E.; Zhang, Y.; Wang, Y.; Kong, W.; Sha, Y.; Tang, W.; Zhang, P.; Wu, Y.; Chen, W.; et al. High Electron Affinity Enables Fast Hole Extraction for Efficient Flexible Inverted Perovskite Solar Cells. *Adv. Energy Mater.* **2020**, *10*, 1903487. [CrossRef]
15. Min, H.; Lee, D.Y.; Kim, J.; Kim, G.; Lee, K.S.; Kim, J.; Paik, M.J.; Kim, Y.K.; Kim, K.S.; Kim, M.G.; et al. Perovskite solar cells with atomically coherent interlayers on SnO_2 electrodes. *Nature* **2021**, *598*, 444–450. [CrossRef] [PubMed]
16. Chen, Y.; Tan, S.; Li, N.; Huang, B.; Niu, X.; Li, L.; Sun, M.; Zhang, Y.; Zhang, X.; Zhu, C.; et al. Self-Elimination of Intrinsic Defects Improves the Low−Temperature Performance of Perovskite Photovoltaics. *Joule* **2020**, *4*, 1961–1976. [CrossRef]
17. Wang, S.; Jiang, Y.; Juarez-Perez, E.J.; Ono, L.K.; Qi, Y. Accelerated degradation of methylammonium lead iodide perovskites induced by exposure to iodine vapour. *Nat. Energy* **2016**, *2*, 16195. [CrossRef]
18. Bisquert, J.; Juarez-Perez, E.J. The Causes of Degradation of Perovskite Solar Cells. *J. Phys. Chem. Lett.* **2019**, *10*, 5889–5891. [CrossRef] [PubMed]
19. Dunfield, S.P.; Bliss, L.; Zhang, F.; Luther, J.M.; Zhu, K.; van Hest, M.F.A.M.; Reese, M.O.; Berry, J.J. From Defects to Degradation: A Mechanistic Understanding of Degradation in Perovskite Solar Cell Devices and Modules. *Adv. Energy Mater.* **2020**, *10*, 1904054. [CrossRef]
20. Conings, B.; Drijkoningen, J.; Gauquelin, N.; Babayigit, A.; D'Haen, J.; D'Olieslaeger, L.; Ethirajan, A.; Verbeeck, J.; Manca, J.; Mosconi, E.; et al. Intrinsic Thermal Instability of Methylammonium Lead Trihalide Perovskite. *Adv. Energy Mater.* **2015**, *5*, 1500477. [CrossRef]
21. Yang, H.; Zhang, J.; Zhang, C.; Chang, J.; Lin, Z.; Chen, D.; Xi, H.; Hao, Y. Effects of Annealing Conditions on Mixed Lead Halide Perovskite Solar Cells and Their Thermal Stability Investigation. *Materials* **2017**, *10*, 837. [CrossRef]
22. Reese, M.O.; Gevorgyan, S.A.; Jørgensen, M.; Bundgaard, E.; Kurtz, S.R.; Ginley, D.S.; Olson, D.C.; Lloyd, M.T.; Morvillo, P.; Katz, E.A.; et al. Consensus stability testing protocols for organic photovoltaic materials and devices. *Sol. Energy Mater. Sol. Cells* **2011**, *95*, 1253–1267. [CrossRef]
23. Kulbak, M.; Cahen, D.; Hodes, G. How Important Is the Organic Part of Lead Halide Perovskite Photovoltaic Cells? Efficient CsPbBr3 Cells. *J. Phys. Chem. Lett.* **2015**, *6*, 2452–2456. [CrossRef] [PubMed]
24. Zhang, J.; Hodes, G.; Jin, Z.; Liu, S. All-inorganic CsPbX3 Perovskite Solar Cells: Progress and Prospects. *Angew. Chem. Int. Ed.* **2019**, *58*, 15596–15618. [CrossRef] [PubMed]
25. Chen, Y.; Li, F.; Zhang, M.; Yang, Z. Recent Progress on Boosting the Perovskite Film Quality of All-Inorganic Perovskite Solar Cells. *Coatings* **2023**, *13*, 281. [CrossRef]
26. Sutton, R.J.; Eperon, G.E.; Miranda, L.; Parrott, E.S.; Kamino, B.A.; Patel, J.B.; Hörantner, M.T.; Johnston, M.B.; Haghighirad, A.A.; Moore, D.T.; et al. Bandgap-Tunable Cesium Lead Halide Perovskites with High Thermal Stability for Efficient Solar Cells. *Adv. Energy Mater.* **2016**, *6*, 1502458. [CrossRef]
27. Guo, Z.; Jena, A.K.; Takei, I.; Kim, G.M.; Kamarudin, M.A.; Sanehira, Y.; Ishii, A.; Numata, Y.; Hayase, S.; Miyasaka, T. VOC Over 1.4 V for Amorphous Tin-Oxide-Based Dopant-Free CsPbI2Br Perovskite Solar Cells. *J. Am. Chem. Soc.* **2020**, *142*, 9725–9734. [CrossRef]
28. Berhe, T.A.; Su, W.-N.; Chen, C.-H.; Pan, C.-J.; Cheng, J.-H.; Chen, H.-M.; Tsai, M.-C.; Chen, L.-Y.; Dubale, A.A.; Hwang, B.-J. Organometal halide perovskite solar cells: Degradation and stability. *Energy Environ. Sci.* **2016**, *9*, 323–356. [CrossRef]
29. Wu, C.; Wang, K.; Feng, X.; Jiang, Y.; Yang, D.; Hou, Y.; Yan, Y.; Sanghadasa, M.; Priya, S. Ultrahigh Durability Perovskite Solar Cells. *Nano Lett.* **2019**, *19*, 1251–1259. [CrossRef]
30. Schloemer, T.H.; Christians, J.A.; Luther, J.M.; Sellinger, A. Doping strategies for small molecule organic hole-transport materials: Impacts on perovskite solar cell performance and stability. *Chem. Sci.* **2019**, *10*, 1904–1935. [CrossRef]
31. Liang, L.; Cai, Y.; Li, X.; Nazeeruddin, M.K.; Gao, P. All that glitters is not gold: Recent progress of alternative counter electrodes for perovskite solar cells. *Nano Energy* **2018**, *52*, 211–238. [CrossRef]
32. Dong, C.; Xu, B.; Liu, D.; Moloney, E.G.; Tan, F.; Yue, G.; Liu, R.; Zhang, D.; Zhang, W.; Saidaminov, M.I. Carbon-based all-inorganic perovskite solar cells: Progress, challenges and strategies toward 20% efficiency. *Mater. Today* **2021**, *50*, 239–258. [CrossRef]
33. Li, W.; Rothmann, M.U.; Liu, A.; Wang, Z.; Zhang, Y.; Pascoe, A.R.; Lu, J.; Jiang, L.; Chen, Y.; Huang, F.; et al. Phase Segregation Enhanced Ion Movement in Efficient Inorganic CsPbIBr2 Solar Cells. *Adv. Energy Mater.* **2017**, *7*, 1700946. [CrossRef]
34. Meng, F.; Liu, A.; Gao, L.; Cao, J.; Yan, Y.; Wang, N.; Fan, M.; Wei, G.; Ma, T. Current progress in interfacial engineering of carbon-based perovskite solar cells. *J. Mater. Chem. A* **2019**, *7*, 8690–8699. [CrossRef]
35. Tress, W. Maximum Efficiency and Open−Circuit Voltage of Perovskite Solar Cells. In *Organic-Inorganic Halide Perovskite Photovoltaics: From Fundamentals to Device Architectures*; Park, N.−G., Grätzel, M., Miyasaka, T., Eds.; Springer International Publishing: Cham, Switzerland, 2016; pp. 53–77.
36. Wang, H.; Liu, H.; Dong, Z.; Li, W.; Zhu, L.; Chen, H. Composition manipulation boosts the efficiency of carbon-based CsPbI3 perovskite solar cells to beyond 14%. *Nano Energy* **2021**, *84*, 105881. [CrossRef]
37. Wang, H.; Liu, H.; Dong, Z.; Song, T.; Li, W.; Zhu, L.; Bai, Y.; Chen, H. Size mismatch induces cation segregation in CsPbI3: Forming energy level gradient and 3D/2D heterojunction promotes the efficiency of carbon-based perovskite solar cells to over 15%. *Nano Energy* **2021**, *89*, 106411. [CrossRef]
38. Singh, A.; Satapathi, S. Advances in Processing Kinetics for All-inorganic Halide Perovskite: Towards Efficient and Thermodynamic Stable Solar Cells. *Adv. Mater. Interfaces* **2022**, *9*, 2200847. [CrossRef]

39. Ding, C.; Zhang, Y.; Liu, F.; Kitabatake, Y.; Hayase, S.; Toyoda, T.; Yoshino, K.; Minemoto, T.; Katayama, K.; Shen, Q. Effect of the conduction band offset on interfacial recombination behavior of the planar perovskite solar cells. *Nano Energy* **2018**, *53*, 17–26. [CrossRef]
40. Su, G.; He, B.; Gong, Z.; Ding, Y.; Duan, J.; Zhao, Y.; Chen, H.; Tang, Q. Enhanced charge extraction in carbon-based all-inorganic CsPbBr3 perovskite solar cells by dual-function interface engineering. *Electrochim. Acta* **2019**, *328*, 135102. [CrossRef]
41. Zhu, W.; Zhang, Z.; Chai, W.; Zhang, Q.; Chen, D.; Lin, Z.; Chang, J.; Zhang, J.; Zhang, C.; Hao, Y. Band Alignment Engineering Towards High Efficiency Carbon-based Inorganic Planar CsPbIBr2 Perovskite Solar Cells. *ChemSusChem* **2019**, *12*, 2318–2325. [CrossRef]
42. Guo, Z.; Zhao, S.; Liu, A.; Kamata, Y.; Teo, S.; Yang, S.; Xu, Z.; Hayase, S.; Ma, T. Niobium Incorporation into CsPbI2Br for Stable and Efficient All-inorganic Perovskite Solar Cells. *ACS Appl. Mater. Interfaces* **2019**, *11*, 19994–20003. [CrossRef]
43. Wang, D.; Li, W.; Li, R.; Sun, W.; Wu, J.; Lan, Z. High−Efficiency Carbon-based CsPbIBr2 Solar Cells with Interfacial Energy Loss Suppressed by a Thin Bulk-Heterojunction Layer. *Sol. RRL* **2021**, *5*, 2100375. [CrossRef]
44. Zhang, J.; Wang, C.; Fu, H.; Gong, L.; He, H.; Fang, Z.; Zhou, C.; Chen, J.; Chao, Z.; Fan, J. Low-temperature preparation achieving 10.95%-efficiency of hole-free and carbon-based all-inorganic CsPbI3 perovskite solar cells. *J. Alloy. Compd.* **2021**, *862*, 158454. [CrossRef]
45. Deng, F.; Li, X.; Lv, X.; Zhou, J.; Chen, Y.; Sun, X.; Zheng, Y.-Z.; Tao, X.; Chen, J.-F. Low-Temperature Processing All-inorganic Carbon-based Perovskite Solar Cells up to 11.78% Efficiency via Alkali Hydroxides Interfacial Engineering. *ACS Appl. Energy Mater.* **2020**, *3*, 401–410. [CrossRef]
46. Zhu, J.; Tang, M.; He, B.; Zhang, W.; Li, X.; Gong, Z.; Chen, H.; Duan, Y.; Tang, Q. Improved charge extraction through interface engineering for 10.12% efficiency and stable CsPbBr3 perovskite solar cells. *J. Mater. Chem. A* **2020**, *8*, 20987–20997. [CrossRef]
47. Liu, J.; Zhu, L.; Xiang, S.; Wang, H.; Liu, H.; Li, W.; Chen, H. Cs−Doped TiO2 Nanorod Array Enhances Electron Injection and Transport in Carbon-based CsPbI3 Perovskite Solar Cells. *ACS Sustain. Chem. Eng.* **2019**, *7*, 16927–16932. [CrossRef]
48. Mi, L.; Zhang, Y.; Chen, T.; Xu, E.; Jiang, Y. Carbon electrode engineering for high efficiency all-inorganic perovskite solar cells. *RSC Adv.* **2020**, *10*, 12298–12303. [CrossRef] [PubMed]
49. Liu, X.; Li, J.; Liu, Z.; Tan, X.; Sun, B.; Xi, S.; Shi, T.; Tang, Z.; Liao, G. Vapor−assisted deposition of CsPbIBr2 films for highly efficient and stable carbon-based planar perovskite solar cells with superior Voc. *Electrochim. Acta* **2020**, *330*, 135266. [CrossRef]
50. Zhu, W.; Zhang, Q.; Chen, D.; Zhang, Z.; Lin, Z.; Chang, J.; Zhang, J.; Zhang, C.; Hao, Y. Intermolecular Exchange Boosts Efficiency of Air-Stable, Carbon-based All-inorganic Planar CsPbIBr2 Perovskite Solar Cells to Over 9%. *Adv. Energy Mater.* **2018**, *8*, 1802080. [CrossRef]
51. Guo, Y.; Zhao, F.; Wang, X.; Tao, J.; Zheng, D.; Jiang, J.; Hu, Z.; Chu, J. Multi−source cation/anion doping towards efficient carbon-based CsPbIBr2 solar cells with superior open voltage up to 1.37 V. *Sol. Energy Mater. Sol. Cells* **2021**, *221*, 110918. [CrossRef]
52. Goldschmidt, V.M. Krystallbau und chemische Zusammensetzung. *Ber. Der Dtsch. Chem. Ges. A B Ser.* **1927**, *60*, 1263–1296. [CrossRef]
53. Travis, W.; Glover, E.N.K.; Bronstein, H.; Scanlon, D.O.; Palgrave, R.G. On the application of the tolerance factor to inorganic and hybrid halide perovskites: A revised system. *Chem. Sci.* **2016**, *7*, 4548–4556. [CrossRef] [PubMed]
54. Ahmad, W.; Khan, J.; Niu, G.; Tang, J. Inorganic CsPbI3 Perovskite−Based Solar Cells: A Choice for a Tandem Device. *Sol. RRL* **2017**, *1*, 1700048. [CrossRef]
55. Stoumpos, C.C.; Malliakas, C.D.; Kanatzidis, M.G. Semiconducting Tin and Lead Iodide Perovskites with Organic Cations: Phase Transitions, High Mobilities, and Near−Infrared Photoluminescent Properties. *Inorg. Chem.* **2013**, *52*, 9019–9038. [CrossRef] [PubMed]
56. Zhou, Y.; Zhang, X.; Lu, X.; Gao, X.; Gao, J.; Shui, L.; Wu, S.; Liu, J.-M. Promoting the Hole Extraction with Co3O4 Nanomaterials for Efficient Carbon-based CsPbI2Br Perovskite Solar Cells. *Sol. RRL* **2019**, *3*, 1800315. [CrossRef]
57. Ding, J.; Duan, J.; Guo, C.; Tang, Q. Toward charge extraction in all-inorganic perovskite solar cells by interfacial engineering. *J. Mater. Chem. A* **2018**, *6*, 21999–22004. [CrossRef]
58. Liang, J.; Han, X.; Yang, J. −H.; Zhang, B.; Fang, Q.; Zhang, J.; Ai, Q.; Ogle, M.M.; Terlier, T.; Martí, A.A.; et al. Defect−Engineering-Enabled High-Efficiency All-inorganic Perovskite Solar Cells. *Adv. Mater.* **2019**, *31*, 1903448. [CrossRef]
59. Duan, J.; Zhao, Y.; Yang, X.; Wang, Y.; He, B.; Tang, Q. Lanthanide Ions Doped CsPbBr3 Halides for HTM-Free 10.14%-Efficiency Inorganic Perovskite Solar Cell with an Ultrahigh Open-Circuit Voltage of 1.594 V. *Adv. Energy Mater.* **2018**, *8*, 1802346. [CrossRef]
60. Xiang, S.; Li, W.; Wei, Y.; Liu, J.; Liu, H.; Zhu, L.; Yang, S.; Chen, H. Natrium Doping Pushes the Efficiency of Carbon-based CsPbI3 Perovskite Solar Cells to 10.7%. *iScience* **2019**, *15*, 156–164. [CrossRef]
61. Meng, X.; Wang, Z.; Qian, W.; Zhu, Z.; Zhang, T.; Bai, Y.; Hu, C.; Xiao, S.; Yang, Y.; Yang, S. Excess Cesium Iodide Induces Spinodal Decomposition of CsPbI2Br Perovskite Films. *J. Phys. Chem. Lett.* **2019**, *10*, 194–199. [CrossRef]
62. Zhu, J.; Liu, Y.; He, B.; Zhang, W.; Cui, L.; Wang, S.; Chen, H.; Duan, Y.; Tang, Q. Efficient interface engineering of N, N′−Dicyclohexylcarbodiimide for stable HTMs−free CsPbBr3 perovskite solar cells with 10.16%-efficiency. *Chem. Eng. J.* **2022**, *428*, 131950. [CrossRef]
63. Yang, Z.; Zhang, G.; Zhang, J.; Pan, Z.; Yang, S.; Liu, B.; Rao, H.; Zhong, X. Synergistic passivation by alkali metal and halogenoid ions for high efficiency HTM-free carbon-based CsPbI2Br solar cells. *Chem. Eng. J.* **2022**, *430*, 133083. [CrossRef]

64. Rakita, Y.; Kedem, N.; Gupta, S.; Sadhanala, A.; Kalchenko, V.; Böhm, M.L.; Kulbak, M.; Friend, R.H.; Cahen, D.; Hodes, G. Low-Temperature Solution-Grown CsPbBr3 Single Crystals and Their Characterization. *Cryst. Growth Des.* **2016**, *16*, 5717–5725. [CrossRef]
65. Correa-Baena, J.-P.; Luo, Y.; Brenner, T.M.; Snaider, J.; Sun, S.; Li, X.; Jensen, M.A.; Hartono, N.T.P.; Nienhaus, L.; Wieghold, S.; et al. Homogenized halides and alkali cation segregation in alloyed organic-inorganic perovskites. *Science* **2019**, *363*, 627–631. [CrossRef] [PubMed]
66. Zhang, S.; Wu, S.; Chen, W.; Zhu, H.; Xiong, Z.; Yang, Z.; Chen, C.; Chen, R.; Han, L.; Chen, W. Solvent engineering for efficient inverted perovskite solar cells based on inorganic CsPbI2Br light absorber. *Mater. Today Energy* **2018**, *8*, 125–133. [CrossRef]
67. Rao, H.; Ye, S.; Gu, F.; Zhao, Z.; Liu, Z.; Bian, Z.; Huang, C. Morphology Controlling of All-inorganic Perovskite at Low Temperature for Efficient Rigid and Flexible Solar Cells. *Adv. Energy Mater.* **2018**, *8*, 1800758. [CrossRef]
68. Chen, H.; Yang, S. Methods and strategies for achieving high-performance carbon-based perovskite solar cells without hole transport materials. *J. Mater. Chem. A* **2019**, *7*, 15476–15490. [CrossRef]
69. Chen, Z.; Dong, Q.; Liu, Y.; Bao, C.; Fang, Y.; Lin, Y.; Tang, S.; Wang, Q.; Xiao, X.; Bai, Y.; et al. Thin single crystal perovskite solar cells to harvest below-bandgap light absorption. *Nat. Commun.* **2017**, *8*, 1890. [CrossRef]
70. Chen, H.; Yang, S. Carbon-based Perovskite Solar Cells without Hole Transport Materials: The Front Runner to the Market? *Adv. Mater.* **2017**, *29*, 1603994. [CrossRef]
71. Zhang, G.; Xie, P.; Huang, Z.; Yang, Z.; Pan, Z.; Fang, Y.; Rao, H.; Zhong, X. Modification of Energy Level Alignment for Boosting Carbon-based CsPbI2Br Solar Cells with 14% Certified Efficiency. *Adv. Funct. Mater.* **2021**, *31*, 2011187. [CrossRef]
72. Ullah, S.; Liu, L.; Yang, S.-E.; Liu, P.; Guo, H.; Chen, Y. A modified hybrid chemical vapor deposition method for the fabrication of efficient $CsPbBr_3$ perovskite solar cells. *J. Phys. D Appl. Phys.* **2021**, *55*, 064001. [CrossRef]
73. Luo, P.; Zhou, Y.; Zhou, S.; Lu, Y.; Xu, C.; Xia, W.; Sun, L. Fast anion-exchange from CsPbI3 to CsPbBr3 via Br2-vapor-assisted deposition for air-stable all-inorganic perovskite solar cells. *Chem. Eng. J.* **2018**, *343*, 146–154. [CrossRef]
74. Bidikoudi, M.; Simal, C.; Stathatos, E. Exploring the Effect of Lewis−Base Additives on the Performance and Stability of Mesoscopic Carbon-Electrode Perovskite Solar Cells. *ACS Appl. Energy Mater.* **2021**, *4*, 8810–8823. [CrossRef]
75. Wang, G.; Liu, J.; Lei, M.; Zhang, W.; Zhu, G. Optimizing the substrate pre-heating and post-annealing temperatures for fabricating high-performance carbon-based CsPbIBr2 inorganic perovskite solar cells. *Electrochim. Acta* **2020**, *349*, 136354. [CrossRef]
76. Yan, J.; Lin, S.; Qiu, X.; Chen, H.; Li, K.; Yuan, Y.; Long, M.; Yang, B.; Gao, Y.; Zhou, C. Accelerated hole-extraction in carbon-electrode based planar perovskite solar cells by moisture-assisted post-annealing. *Appl. Phys. Lett.* **2019**, *114*, 103503. [CrossRef]
77. Liu, L.; Yang, S.-E.; Liu, P.; Chen, Y. High-quality and full-coverage CsPbBr3 thin films via electron beam evaporation with post−annealing treatment for all-inorganic perovskite solar cells. *Sol. Energy* **2022**, *232*, 320–327. [CrossRef]
78. Zhang, L.; Chen, S.; Zeng, J.; Jiang, Z.; Ai, Q.; Zhang, X.; Hu, B.; Wang, X.; Yang, S.; Xu, B. Inkjet-Printing Controlled Phase Evolution Boosts the Efficiency of Hole Transport Material Free and Carbon-based CsPbBr3 Perovskite Solar Cells Exceeding 9%. *Energy Environ. Mater.* **2022**, e12543. [CrossRef]
79. Haruta, Y.; Ikenoue, T.; Miyake, M.; Hirato, T. One-Step Coating of Full-Coverage CsPbBr3 Thin Films via Mist Deposition for All-inorganic Perovskite Solar Cells. *ACS Appl. Energy Mater.* **2020**, *3*, 11523–11528. [CrossRef]
80. Zhang, Z.; Ba, Y.; Chen, D.; Ma, J.; Zhu, W.; Xi, H.; Chen, D.; Zhang, J.; Zhang, C.; Hao, Y. Generic water-based spray-assisted growth for scalable high-efficiency carbon-electrode all-inorganic perovskite solar cells. *iScience* **2021**, *24*, 103365. [CrossRef]
81. Mastrikov, Y.A.; Chuklina, N.G.; Sokolov, M.N.; Popov, A.I.; Gryaznov, D.V.; Kotomin, E.A.; Maier, J. Small radius electron and hole polarons in PbX2 (X = F, Cl, Br) crystals: A computational study. *J. Mater. Chem. C* **2021**, *9*, 16536–16544. [CrossRef]
82. Popov, A.I.; Kotomin, E.A.; Maier, J. Analysis of self-trapped hole mobility in alkali halides and metal halides. *Solid State Ion.* **2017**, *302*, 3–6. [CrossRef]
83. Slotcavage, D.J.; Karunadasa, H.I.; McGehee, M.D. Light-Induced Phase Segregation in Halide−Perovskite Absorbers. *ACS Energy Lett.* **2016**, *1*, 1199–1205. [CrossRef]
84. Ball, J.M.; Petrozza, A. Defects in perovskite-halides and their effects in solar cells. *Nat. Energy* **2016**, *1*, 16149. [CrossRef]
85. Wang, Y.; Dar, M.I.; Ono, L.K.; Zhang, T.; Kan, M.; Li, Y.; Zhang, L.; Wang, X.; Yang, Y.; Gao, X.; et al. Thermodynamically stabilized β-CsPbI3-based perovskite solar cells with efficiencies >18%. *Science* **2019**, *365*, 591–595. [CrossRef] [PubMed]
86. Dong, C.; Han, X.; Zhao, Y.; Li, J.; Chang, L.; Zhao, W. A Green Anti−Solvent Process for High Performance Carbon-based CsPbI2Br All-inorganic Perovskite Solar Cell. *Sol. RRL* **2018**, *2*, 1800139. [CrossRef]
87. Yang, S.; Zhao, H.; Han, Y.; Duan, C.; Liu, Z.; Liu, S. Europium and Acetate Co−doping Strategy for Developing Stable and Efficient CsPbI2Br Perovskite Solar Cells. *Small* **2019**, *15*, 1904387. [CrossRef] [PubMed]
88. Liang, J.; Wang, C.; Wang, Y.; Xu, Z.; Lu, Z.; Ma, Y.; Zhu, H.; Hu, Y.; Xiao, C.; Yi, X.; et al. All-inorganic Perovskite Solar Cells. *J. Am. Chem. Soc.* **2016**, *138*, 15829–15832. [CrossRef]
89. Duan, J.; Zhao, Y.; He, B.; Tang, Q. High-Purity Inorganic Perovskite Films for Solar Cells with 9.72% Efficiency. *Angew. Chem. Int. Ed.* **2018**, *57*, 3787–3791. [CrossRef]
90. Bu, F.; He, B.; Ding, Y.; Li, X.; Sun, X.; Duan, J.; Zhao, Y.; Chen, H.; Tang, Q. Enhanced energy level alignment and hole extraction of carbon electrode for air-stable hole-transporting material-free CsPbBr3 perovskite solar cells. *Sol. Energy Mater. Sol. Cells* **2020**, *205*, 110267. [CrossRef]

91. Guo, R.; Zhao, Y.; Deng, Q.; Zhang, Y.; Wu, Z.; Duan, Y.; Zhang, W.; Shen, Y.; Shao, G. Energy level matching between transparent conducting electrodes and the electronic transport layer to enhance performance of all-inorganic CsPbBr3 solar cells. *Vacuum* **2022**, *200*, 111028. [CrossRef]
92. Yao, X.; He, B.; Zhu, J.; Ti, J.; Cui, L.; Tui, R.; Wei, M.; Chen, H.; Duan, J.; Duan, Y.; et al. Tailoring type-II all-in-one buried interface for 1.635V-voltage, all-inorganic CsPbBr3 perovskite solar cells. *Nano Energy* **2022**, *96*, 107138. [CrossRef]
93. Wang, S.; Cao, F.; Sun, W.; Wang, C.; Yan, Z.; Wang, N.; Lan, Z.; Wu, J. A green Bi-Solvent system for processing high-quality CsPbBr3 films in efficient all-inorganic perovskite solar cells. *Mater. Today Phys.* **2022**, *22*, 100614. [CrossRef]
94. Teng, P.; Han, X.; Li, J.; Xu, Y.; Kang, L.; Wang, Y.; Yang, Y.; Yu, T. Elegant Face−Down Liquid-Space-Restricted Deposition of CsPbBr3 Films for Efficient Carbon-based All-inorganic Planar Perovskite Solar Cells. *ACS Appl. Mater. Interfaces* **2018**, *10*, 9541–9546. [CrossRef] [PubMed]
95. Wang, D.; Li, W.; Du, Z.; Li, G.; Sun, W.; Wu, J.; Lan, Z. Highly Efficient CsPbBr3 Planar Perovskite Solar Cells via Additive Engineering with NH4SCN. *ACS Appl. Mater. Interfaces* **2020**, *12*, 10579–10587. [CrossRef]
96. Liu, X.; Tan, X.; Liu, Z.; Ye, H.; Sun, B.; Shi, T.; Tang, Z.; Liao, G. Boosting the efficiency of carbon-based planar CsPbBr3 perovskite solar cells by a modified multistep spin−coating technique and interface engineering. *Nano Energy* **2019**, *56*, 184–195. [CrossRef]
97. Zhang, X.; Jin, Z.; Zhang, J.; Bai, D.; Bian, H.; Wang, K.; Sun, J.; Wang, Q.; Liu, S.F. All-Ambient Processed Binary CsPbBr3-CsPb2Br5 Perovskites with Synergistic Enhancement for High-Efficiency Cs-Pb-Br-Based Solar Cells. *ACS Appl. Mater. Interfaces* **2018**, *10*, 7145–7154. [CrossRef]
98. Tong, G.; Chen, T.; Li, H.; Qiu, L.; Liu, Z.; Dang, Y.; Song, W.; Ono, L.K.; Jiang, Y.; Qi, Y. Phase transition induced recrystallization and low surface potential barrier leading to 10.91%-efficient CsPbBr3 perovskite solar cells. *Nano Energy* **2019**, *65*, 104015. [CrossRef]
99. Jiang, L.; Peng, Y.; Xiang, T.; Liu, Y.; Xu, M.; Wang, J.; Tremblay, P.-L.; Zhang, T. A counter electrode modified with renewable carbonized biomass for an all-inorganic CsPbBr3 perovskite solar cell. *J. Alloy. Compd.* **2022**, *902*, 163725. [CrossRef]
100. Liu, J.; He, Q.; Bi, J.; Lei, M.; Zhang, W.; Wang, G. Remarkable quality improvement of CsPbIBr2 perovskite film by cellulose acetate addition for efficient and stable carbon-based inorganic perovskite solar cells. *Chem. Eng. J.* **2021**, *424*, 130324. [CrossRef]
101. Liu, J.; Lei, M.; Zhang, W.; Wang, G. A multifunctional CuSCN interlayer in carbon electrode-based CsPbIBr2 all-inorganic perovskite solar cells for boosting the efficiency and stability. *Sustain. Energy Fuels* **2020**, *4*, 4249–4256. [CrossRef]
102. Yang, S.; Wang, L.; Gao, L.; Cao, J.; Han, Q.; Yu, F.; Kamata, Y.; Zhang, C.; Fan, M.; Wei, G.; et al. Excellent Moisture Stability and Efficiency of Inverted All-inorganic CsPbIBr2 Perovskite Solar Cells through Molecule Interface Engineering. *ACS Appl. Mater. Interfaces* **2020**, *12*, 13931–13940. [CrossRef]
103. Liang, J.; Zhao, P.; Wang, C.; Wang, Y.; Hu, Y.; Zhu, G.; Ma, L.; Liu, J.; Jin, Z. CsPb0.9Sn0.1IBr2 Based All-inorganic Perovskite Solar Cells with Exceptional Efficiency and Stability. *J. Am. Chem. Soc.* **2017**, *139*, 14009–14012. [CrossRef] [PubMed]
104. Zhou, Q.; Tang, S.; Yuan, G.; Zhu, W.; Huang, Y.; Li, S.; Lin, M. Tailored graphene quantum dots to passivate defects and accelerate charge extraction for all-inorganic CsPbIBr2 perovskite solar cells. *J. Alloy. Compd.* **2022**, *895*, 162529. [CrossRef]
105. Wang, H.; Sun, J.; Gu, Y.; Xu, C.; Lu, Y.; Hu, J.; Chen, T.; Zhu, C.; Luo, P. Solvent-engineering-processed CsPbIBr2 inorganic perovskite solar cells with efficiency of ∼11%. *Sol. Energy Mater. Sol. Cells* **2022**, *238*, 111640. [CrossRef]
106. Ma, Q.; Huang, S.; Wen, X.; Green, M.A.; Ho−Baillie, A.W.Y. Hole Transport Layer Free Inorganic CsPbIBr2 Perovskite Solar Cell by Dual Source Thermal Evaporation. *Adv. Energy Mater.* **2016**, *6*, 1502202. [CrossRef]
107. Lau, C.F.J.; Deng, X.; Ma, Q.; Zheng, J.; Yun, J.S.; Green, M.A.; Huang, S.; Ho−Baillie, A.W.Y. CsPbIBr2 Perovskite Solar Cell by Spray-Assisted Deposition. *ACS Energy Lett.* **2016**, *1*, 573–577. [CrossRef]
108. Guo, Y.; Yin, X.; Liu, J.; Wen, S.; Wu, Y.; Que, W. Inorganic CsPbIBr2-Based Perovskite Solar Cells: Fabrication Technique Modification and Efficiency Improvement. *Sol. RRL* **2019**, *3*, 1900135. [CrossRef]
109. Zhang, Q.; Zhu, W.; Chen, D.; Zhang, Z.; Lin, Z.; Chang, J.; Zhang, J.; Zhang, C.; Hao, Y. Light Processing Enables Efficient Carbon-based, All-inorganic Planar CsPbIBr2 Solar Cells with High Photovoltages. *ACS Appl. Mater. Interfaces* **2019**, *11*, 2997–3005. [CrossRef]
110. Zhu, W.; Chai, W.; Deng, M.; Chen, D.; Chen, D.; Zhang, J.; Zhang, C.; Hao, Y. Flux−mediated growth strategy enables low−temperature fabrication of high−efficiency all-inorganic CsPbIBr2 perovskite solar cells. *Electrochim. Acta* **2020**, *330*, 135325. [CrossRef]
111. Zhu, W.; Chai, W.; Chen, D.; Xi, H.; Chen, D.; Chang, J.; Zhang, J.; Zhang, C.; Hao, Y. Recycling of FTO/TiO_2 Substrates: Route toward Simultaneously High-performance and Cost−Efficient Carbon-based, All-inorganic $CsPbIBr_2$ Solar Cells. *ACS Appl. Mater. Interfaces* **2020**, *12*, 4549–4557. [CrossRef]
112. Nam, J.K.; Jung, M.S.; Chai, S.U.; Choi, Y.J.; Kim, D.; Park, J.H. Unveiling the Crystal Formation of Cesium Lead Mixed-Halide Perovskites for Efficient and Stable Solar Cells. *J. Phys. Chem. Lett.* **2017**, *8*, 2936–2940. [CrossRef]
113. Lin, J.; Lai, M.; Dou, L.; Kley, C.S.; Chen, H.; Peng, F.; Sun, J.; Lu, D.; Hawks, S.A.; Xie, C.; et al. Thermochromic halide perovskite solar cells. *Nat. Mater.* **2018**, *17*, 261–267. [CrossRef] [PubMed]
114. Chen, C.-Y.; Lin, H.-Y.; Chiang, K.-M.; Tsai, W.-L.; Huang, Y.-C.; Tsao, C.-S.; Lin, H.-W. All-Vacuum-Deposited Stoichiometrically Balanced Inorganic Cesium Lead Halide Perovskite Solar Cells with Stabilized Efficiency Exceeding 11%. *Adv. Mater.* **2017**, *29*, 1605290. [CrossRef] [PubMed]
115. Lee, D.S.; Ki, M.J.; Lee, H.J.; Park, J.K.; Hong, S.Y.; Kim, B.W.; Heo, J.H.; Im, S.H. Fully Scalable and Stable CsPbI2Br Solar Cells Realized by an All-Spray-Coating Process. *ACS Appl. Mater. Interfaces* **2022**, *14*, 7926–7935. [CrossRef]

116. Lv, J.; Zhao, W.; Li, W.; Yu, J.; Zhang, M.; Han, X.; Tanaka, T. Defect healing via a gradient cooling strategy for efficient all-inorganic perovskite solar cells. *J. Mater. Chem. C* **2022**, *10*, 4276–4285. [CrossRef]
117. Fatima, K.; Haider, M.I.; Bashir, A.; Qamar, S.; Qureshi, A.A.; Akhter, Z.; Sultan, M. Surface modification of CsPbI2Br for improved performance of inorganic perovskite solar cells. *Phys. E Low Dimens. Syst. Nanostructures* **2022**, *142*, 115265. [CrossRef]
118. Jeon, N.J.; Noh, J.H.; Kim, Y.C.; Yang, W.S.; Ryu, S.; Seok, S.I. Solvent engineering for high-performance inorganic-organic hybrid perovskite solar cells. *Nat. Mater.* **2014**, *13*, 897–903. [CrossRef]
119. Liu, C.; Wu, M.; Wu, Y.; Wang, D.; Zhang, T. Efficient all-inorganic CsPbI2Br perovskite solar cell with carbon electrode by revealing crystallization kinetics and improving crystal quality. *J. Power Sour.* **2020**, *447*, 227389. [CrossRef]
120. Xu, X.; Qin, W.; Liu, S.; Xing, C.; Ge, G.; Wang, D.; Zhang, T. Low temperature-processed stable and high-efficiency carbon-based CsPbI2Br perovskite solar cells by additive strategy. *Org. Electron.* **2022**, *103*, 106463. [CrossRef]
121. Zhu, W.; Ma, J.; Chai, W.; Han, T.; Chen, D.; Xie, X.; Liu, G.; Dong, P.; Xi, H.; Chen, D.; et al. Intermediate Phase-Assisted Sequential Deposition toward 15.24%-Efficiency Carbon-Electrode Cspbi2br Perovskite Solar Cells. *Solar RRL* **2022**, *6*, 2200020. [CrossRef]
122. Tan, S.; Shi, J.; Yu, B.; Zhao, W.; Li, Y.; Li, Y.; Wu, H.; Luo, Y.; Li, D.; Meng, Q. Inorganic Ammonium Halide Additive Strategy for Highly Efficient and Stable CsPbI3 Perovskite Solar Cells. *Adv. Funct. Mater.* **2021**, *31*, 2010813. [CrossRef]
123. Fan, Y.; Wang, X.; Miao, Y.; Zhao, Y. The Chemical Design in High-performance Lead Halide Perovskite: Additive vs Dopant? *J. Phys. Chem. Lett.* **2021**, *12*, 11636–11644. [CrossRef] [PubMed]
124. Eperon, G.E.; Paternò, G.M.; Sutton, R.J.; Zampetti, A.; Haghighirad, A.A.; Cacialli, F.; Snaith, H.J. Inorganic caesium lead iodide perovskite solar cells. *J. Mater. Chem. A* **2015**, *3*, 19688–19695. [CrossRef]
125. Wang, Q.; Zheng, X.; Deng, Y.; Zhao, J.; Chen, Z.; Huang, J. Stabilizing the α−Phase of CsPbI3 Perovskite by Sulfobetaine Zwitterions in One-Step Spin-Coating Films. *Joule* **2017**, *1*, 371–382. [CrossRef]
126. Wang, P.; Zhang, X.; Zhou, Y.; Jiang, Q.; Ye, Q.; Chu, Z.; Li, X.; Yang, X.; Yin, Z.; You, J. Solvent-controlled growth of inorganic perovskite films in dry environment for efficient and stable solar cells. *Nat. Commun.* **2018**, *9*, 2225. [CrossRef] [PubMed]
127. Xiang, S.; Fu, Z.; Li, W.; Wei, Y.; Liu, J.; Liu, H.; Zhu, L.; Zhang, R.; Chen, H. Highly Air−Stable Carbon-based α-CsPbI3 Perovskite Solar Cells with a Broadened Optical Spectrum. *ACS Energy Lett.* **2018**, *3*, 1824–1831. [CrossRef]
128. Wang, H.; Liu, H.; Dong, Z.; Wei, X.; Song, Y.; Li, W.; Zhu, L.; Bai, Y.; Chen, H. Extracting ammonium halides by solvent from the hybrid perovskites with various dimensions to promote the crystallization of CsPbI3 perovskite. *Nano Energy* **2022**, *94*, 106925. [CrossRef]
129. Yonezawa, K.; Yamamoto, K.; Shahiduzzaman, M.; Furumoto, Y.; Hamada, K.; Ripolles, T.S.; Karakawa, M.; Kuwabara, T.; Takahashi, K.; Hayase, S.; et al. Annealing effects on $CsPbI_3$-based planar heterojunction perovskite solar cells formed by vacuum deposition method. *Jpn. J. Appl. Phys.* **2017**, *56*, 04CS11. [CrossRef]
130. Yuan, J.; Bi, C.; Wang, S.; Guo, R.; Shen, T.; Zhang, L.; Tian, J. Spray-Coated Colloidal Perovskite Quantum Dot Films for Highly Efficient Solar Cells. *Adv. Funct. Mater.* **2019**, *29*, 1906615. [CrossRef]
131. Lin, Z.; Folgueras, M.C.; Le, H.K.D.; Gao, M.; Yang, P. Laser-accelerated phase transformation in cesium lead iodide perovskite. *Matter* **2022**, *5*, 1455–1465. [CrossRef]
132. Gu, X.; Lai, X.; Zhang, Y.; Wang, T.; Tan, W.L.; McNeill, C.R.; Liu, Q.; Sonar, P.; He, F.; Li, W.; et al. Organic Solar Cell with Efficiency Over 20% and VOC Exceeding 2.1 V Enabled by Tandem with All-inorganic Perovskite and Thermal Annealing-Free Process. *Adv. Sci.* **2022**, *9*, 2200445. [CrossRef]

Disclaimer/Publisher's Note: The statements, opinions and data contained in all publications are solely those of the individual author(s) and contributor(s) and not of MDPI and/or the editor(s). MDPI and/or the editor(s) disclaim responsibility for any injury to people or property resulting from any ideas, methods, instructions or products referred to in the content.